Quaternary slip-rates probabilistic estimation for the Northern Apennines frontal thrust in the Po Plain (Northern Italy) by integrating surface and subsurface data

F.E. Maesano [a,*], C. Zuffetti [b], A. Abbate [a,c], C. D'Ambrogi [d], R. Bersezio [b]

[a] *Istituto Nazionale di Geofisica e Vulcanologia, Rome, Italy*
[b] *Dipartimento di Scienze della Terra, Università degli Studi di Milano, via Mangiagalli 34, 20133 Milano, Italy*
[c] *Dipartimento di Matematica e Geoscienze, Università di Trieste, Trieste, Italy*
[d] *Istituto Superiore per la Protezione e la Ricerca Ambientale, Dip. Servizio Geologico d'Italia, Rome, Italy*

A B S T R A C T

The Northern Apennines thrust front in the Po basin exhibits active blind thrusts and associated anticlines, with some anticline crests either emerging or shallowly buried beneath late Pleistocene continental deposits. This study focuses on the outcropping San Colombano Structure and its buried neighbouring Casalpusterlengo-Zorlesco Structure, representing thrust-controlled anticlines in the central part of the Po basin. We reconstruct the Pleistocene evolution of these anticlines by integrating previously published surface geological maps and subsurface geological constraints from geophysical data and boreholes. We performed a trishear inversion of the deformation observed after the decompaction of the sediments. We used the solutions of the trishear inversion to compute the probabilistic distribution of slip rates over distinct time intervals. Our findings align with previous estimations of long-term slip rates in the Po Plain during the Quaternary, revealing rates of approximately 0.63 mm/yr and 0.53 mm/yr over the past 2.4 Myr for the San Colombano and Casalpusterlengo-Zorlesco Structures, respectively. The analysis of stratigraphic markers unveils a general decrease in faults activity during the Pleistocene, with slip rates around 0.2–0.3 mm/yr in the last 0.3 Myr, along with a diverse evolution of the thrust faults governing the two anticlines. Specifically, the activity rates of the San Colombano Structure supersede that of the Casalpusterlengo-Zorlesco Structure during the Middle to Late Pleistocene, implying an out-of-sequence propagation of the San Colombano ramp-anticline in the Late Pleistocene along an oblique right-lateral transfer zone. Incorporating a probabilistic approach in slip rates calculation provides a more comprehensive handling of uncertainties. This attribute is pivotal in seismic hazard assessment analyses and understanding complex fault systems' tectonic evolution.

1. Introduction

The frontal portions of active contractional orogens are commonly characterised by the association of thrusts and related anticlines and synclines (i.e., fold-and-thrust belts), in some places controlled by blind reverse faults but with significant exposure of the fold structure at the surface (e.g., in the Zagros fold-and-thrust belt, Berberian, 1995; Doski, 2021; Los Angeles Basin, Myers et al., 2003). However, in other places, the combination of slow tectonic and high sedimentation rates may lead to a generally flat topography where the folds and faults are mostly buried under a sedimentary cover, even if they are still active. One of the best examples of this structural situation is the thrust front of the Northern Apennines and Southern Alps in Italy (Fig. 1-A, Fig. 1-B), which is buried below the marine and alluvial deposits of the Po Plain (Toscani et al., 2009).

The outermost thrusts of the Northern Apennines show subtle geological and geomorphological evidence of Quaternary activity highlighted by the control on the modern drainage pattern (Burrato et al., 2012, 2003; Maestrelli et al., 2018) and by the analysis of subsurface data (e.g., seismic reflection profiles and well data) (Fig. 1-C, Fig. 1-D). Subsurface geological and geophysical data show evidence of unconformities in the stratigraphic succession and mild folding above the tip of the buried thrusts (Bresciani and Perotti, 2014; Campo et al., 2020; Maesano et al., 2015; Maestrelli et al., 2018, Fig. 1-D).

---

* Corresponding author at: Istituto Nazionale di Geofisica e Vulcanologia, Via di Vigna Murata 605, 00143 Rome, Italy.
E-mail address: francesco.maesano@ingv.it (F.E. Maesano).

The San Colombano hill, located in the central part of the Po Plain, represents one noticeable exception to the buried characteristic of the Northern Apennines front; it is an isolated relief where the Miocene succession is directly exposed and where the Pleistocene deposits are mainly related to alluvial terraces that have recorded the progressive uplift of the structure (Zuffetti and Bersezio, 2021). For this reason, the San Colombano hill represents an interesting place for attempting a reconstruction of the Quaternary tectonic history and to make a comparison with the previous estimates of the Quaternary slip rates in the Po Plain (Boccaletti et al., 2011; Maesano et al., 2015; Panara et al., 2021).

Previous computation of tectonic slip rates on the faults of the Po Plain relies mainly on subsurface geophysical evidence due to the absence of any surface geological record, with few exceptions on the foothills of the Northern Apennines (Ponza et al., 2010; Gunderson et al., 2013, 2018; Maestrelli et al., 2018) and on isolated reliefs of the Southern Alps (Livio et al., 2009). The difficulties in recognising the

geological markers of the present-day activity of the thrust front were at the core of a long-lasting debate on the seismotectonics of Northern Italy. The Po Plain was affected by significant earthquakes in the past (Rovida et al., 2022), including the 2012 seismic sequence (Malagnini et al., 2012), which indicates the present-day activity of the outer front of the Northern Apennines. This seismic sequence affected the frontal part of the Ferrara-Romagna arc (Fig. 1-B) - a densely populated area with extensive industrial facilities - with two mainshocks (Mw 6.1 and Mw 5.9) in ten days. The two mainshocks ruptured two buried thrust ramps with a maximum slip of 0.8 m (Bonini et al., 2014; Improta et al., 2023). Recently, in November 2022, the offshore portion of the Northern Apennines thrust front in the Pesaro area was also affected by a significant seismic sequence, which started with an Mw 5.5 earthquake nucleated on one of the outermost frontal thrusts of the Northern Apennines (Maesano et al., 2023).

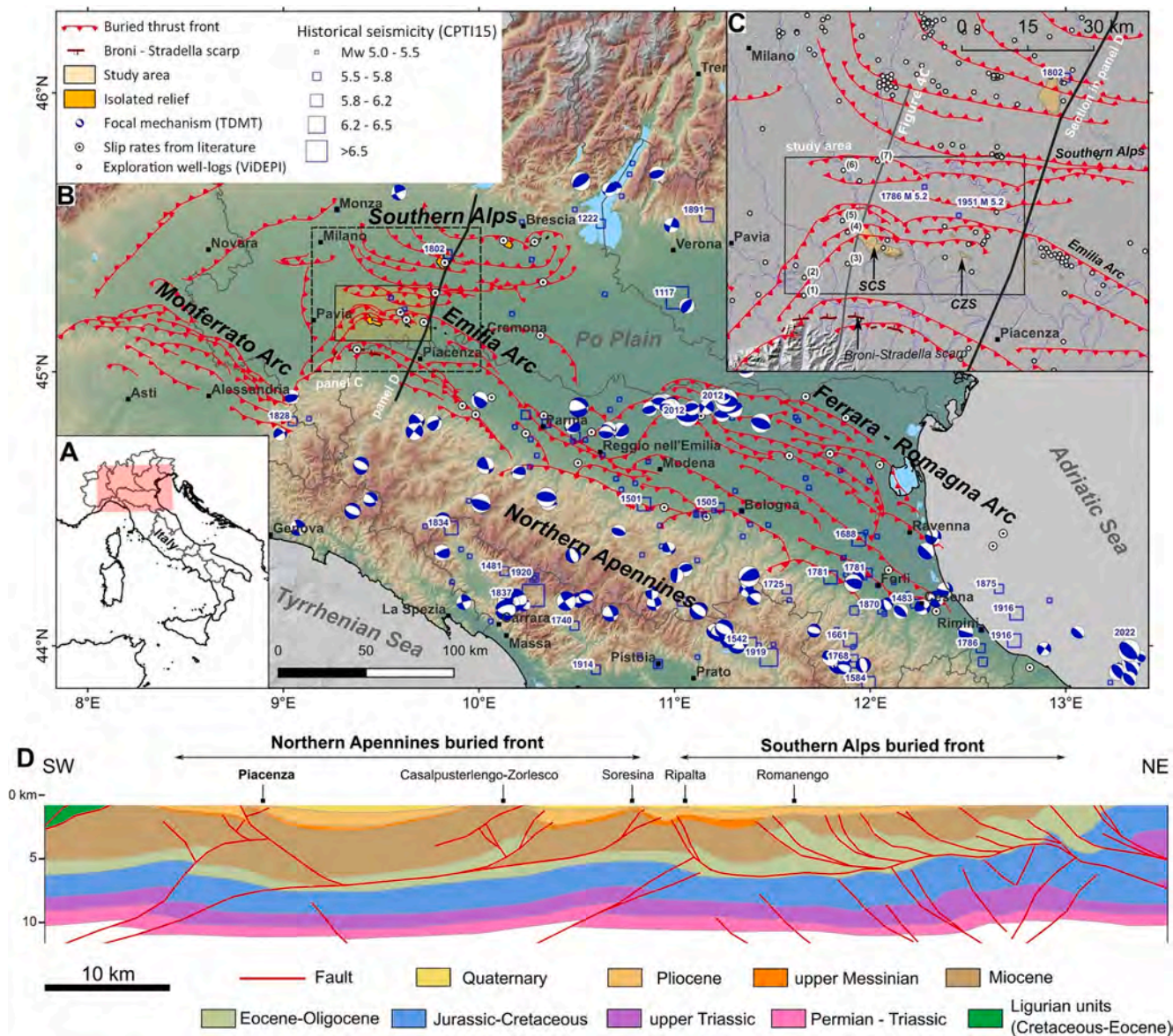Instrumental seismicity in the Po Plain can be associated to faults of

Fig. 1. A) Location map of the study area (rectangular frame). B) Structural and seismotectonic framework of the Po foreland basin (Northern Italy). Dashed black line: frame of Panel C. Solid black line: trace of the regional geological Section of Panel D; TDMT: Time Domain Moment Tensor (Scognamiglio et al., 2006); historical seismicity from CPTI15 (Rovida et al., 2022); fault traces modified from Rossi et al. (2015); slip rates from literature collected by Panara et al. (2021). C) Close-up view of the study area. Production/exploration wells from ViDEPI used for the interpretation of Fig. 3-B: (1) Stradella 1, (2) Belgioioso 1, (3) S. Cristina 1, (4) Inverno 1, (5) Villanterio 1, (6) Salerano 1, (7) Cornegliano 15. Broni-Stradella scarp from Benedetti et al., (2003); Digital Elevation Model EU-DEM v.1.1, Copernicus. D) Geological Section crossing the Apennines Emilia thrust front, modified from Fantoni and Franciosi (2010).

different structural domains. The shallowest earthquakes (<15 km, magnitude up to 5.9, CLASS catalogue, Latorre et al., 2023) can be related to the activity of the thrust fronts of both the Alps and the Apennines. Shallow seismicity concentrates along the Ferrara outer thrust front and in the Parma-Reggio Emilia area. Farther west, seismic activity is weaker. Deeper earthquakes (15–50 km, magnitude up to 5.1, CLASS catalogue, Latorre et al., 2023) are widespread in the Po Plain. These events are associated with inherited and/or transverse faults in the foreland and the inner sector of the Northern Apennines related to the deeper ramp of the Apennines subduction system (Vannoli et al., 2015).

The strongest known historical earthquake in the Po Plain occurred in 1117, south of Verona (Fig. 1-B), with an estimated magnitude of 6.5 (Guidoboni et al., 2005). In the central portion of the Po Plain, the strongest historical earthquake reported by the catalogues occurred in 1802 (Valle dell'Oglio earthquake, Locati et al., 2022; Rovida et al., 2022) with an estimated magnitude of 5.6 and hypocentre depth of 11 km (Sbarra et al., 2023) and located ca. 20 km northeast of the area studied in this work. Within the study area, historical catalogues (Rovida et al., 2022) show the presence of only two M > 5.0 seismic events in 1786 (M 5.2) and 1951 (M 5.2) (Fig. 1-C). The latter earthquake was estimated to be related to a deep source (44 km) based on the macro-seismic effects calibrated with the observation obtained from the instrumental seismicity in the Po Plain (Sbarra et al., 2019).

The significant exposure of the central Po Plain in terms of population density and industrial infrastructures is one of the critical reasons for better documenting the geometry and the tectonic rates of the faults within this area. Estimating the tectonic deformation rates during the Quaternary is a primary input for the seismic hazard assessment at the national (Meletti et al., 2021; Visini et al., 2021) and European level (Danciu et al., 2022). Previous estimates of the slip rates of the Northern Apennines front are in the order of 0.1–1.5 mm/yr, with generally lower values in the western sector than in the eastern sector (Panara et al., 2021 and references therein).

In this work, we focus on the outcropping San Colombano structure (SCS) and, to the east, the adjacent buried Casalpusterlengo-Zorlesco structure (CZS), two segments of the Apennines Emilia Arc (Fig. 1-B, 1-C). We use a combination of detailed surface mapping of unconformities and fluvial terraces from previous works (Zuffetti et al., 2018b; Zuffetti et al., 2018a; Zuffetti et al., 2018c), analysis of shallow wells and geoelectric surveys (Mele et al., 2018; Zuffetti and Bersezio, 2021), and interpretation of subsurface seismic reflection profiles (D'Ambrogi et al., 2023; ViDEPI database, www.videpi.com). The analysis allows us to assess the slip rates associated with the Quaternary evolution of the thrusts controlling the anticlines' development in their outcropping and buried parts. The results highlight variations in the growth of the two adjacent anticlines and the spatial-temporal partitioning of the deformation along the thrust front. Quantitatively estimating the deformation history along adjacent faults may provide helpful insight into better-constrained seismic hazard assessment studies.

2. Geological framework of the Po Basin

The Po alluvial plain in Northern Italy elongates WNW-to-ESE between the opposite fronts of two mountain ranges, the Southern Alps to the north and the Northern Apennines to the south. Since the Late Miocene, this region represented the foreland of the active Northern Apennines fold-and-thrust belt. The foreland was characterised by paleogeographic structural highs that segmented the Northern Apennines front into three main arcs (Monferrato, Emilia and Ferrara-Romagna Arcs, from W to E, respectively; Carminati and Doglioni, 2012; Livani et al., 2018), propagated N- and NE-wards, locally reaching the buried frontal thrusts of the Southern Alps (Fig. 1) and controlling subsidence-sedimentation patterns (Bigi et al., 1992; Carminati et al., 2003; Fantoni et al., 2004).

The interference between the two chains contributed to buttressing the foreland propagation of the Apennines thrusts in the central Po Plain, differently from its eastern prolongation toward the Adriatic foredeep (Ghielmi et al., 2013). Even if both thrust belts are still active (Devoti et al., 2011), the Quaternary subsidence pattern of the southern Po basin is mainly controlled by the activity of the northernmost, buried, and blind Apennines structures (Carminati and Doglioni, 2012).

The regional cross-sections proposed by Fantoni and Franciosi (2010) suggest that ramp thrusts characterise the Outer Emilia Arc detached at the base of the Oligocene stratigraphic units and that have cumulated 5700 m of total offset from their age of inception (Fig. 1-D). The Outer Emilia Arc was already structured in the Early Pliocene (Ghielmi et al., 2013; Ghielmi et al., 2010), and its initial activity has been ascribed to the Messinian pre-evaporitic time (Amadori et al., 2019).

The Outer Emilia Arc is one of the primary seismogenic sources of N-Italy (DISS Working Group, 2021), for which Maesano et al. (2015) proposed a cumulative slip rate of 0.5 mm/yr over the past 1.8 Myr and depths between 2 and 7 km. To the South of the study area, late Quaternary uplift rates of 0.3 mm/yr were inferred on the Broni-Stradella scarp by Benedetti et al. (Benedetti et al., 2003; Fig. 1-C) and interpreted as part of a regional thrust running along the Northern Apennines (Tibaldi et al., 2023).

Quaternary regional tectonics at the Po Plain-Apennines hinge has been dominated by northward thrusting and folding, with local transpression along lateral ramps and deeper reactivation of the Southern Alps thrusts (Bresciani and Perotti, 2014; Burrato et al., 2003; Maesano et al., 2015; Maestrelli et al., 2018), while Zuffetti and Bersezio (2020) documented secondary extensional faulting in the San Colombano hill. The latter belongs to a set of Quaternary intra-basin reliefs emerging above the average elevation of the alluvial plain (Desio, 1965) over the culmination of the deep ramp folds of the Apennines thrust belts.

The Po basin infill is >8 km thick in the depocenter and thins and wedges out toward the northern and southern basin margins and toward the intra-basin isolated reliefs. It consists of a diachronic mega-regressive sequence of Miocene-Pliocene marine units, then Lower Pleistocene shallow marine to alluvial-deltaic deposits, followed by Middle–Upper Pleistocene alluvial and glacial-fluvial units (Ghielmi et al., 2013). The Quaternary sedimentary succession may reach a thickness of >1 km in the main depocenters (Fig. 1-D, Fantoni and Franciosi, 2010; Amadori et al., 2019).

The subsurface Quaternary regional chronostratigraphic dataset relies on magnetostratigraphic interpretations and biostratigraphy from sparse wells in the northern Po Plain (Muttoni et al., 2003), correlated southwards through regional seismic profiles. Industrial seismic data through the basin depocenter show that four major angular unconformities, consequent to the major Miocene-Pleistocene Apennines compressive tectonic stages (Latest Tortonian, Intra-Messinian, Intra-Zanclean, and Gelasian; Ghielmi et al., 2013), bound the highest-rank sequences forming the Mio-Pleistocene stratigraphic succession of the central Po basin. These unconformable boundaries become too close toward the Po basin margins to be confidently traced by seismic lines and deep wells alone in the subsurface.

Relying on down-tracing from geological maps and outcrop-borehole correlations in the southern margin of the central Po Plain, Zuffetti and Bersezio (2021) described four main unconformable boundaries above the Gelasian unconformity (named Intra-Calabrian "U1", Early-Middle Pleistocene "U2", Middle-Late Pleistocene "U3", and Latest Pleistocene-Holocene "U4" unconformities).

Although the interaction between Quaternary sedimentation and faulting is known, no detailed documentation exists on its quantification, especially during its Pleistocene evolution. The present study focuses on a 450 km² wide area at the Po Plain-Apennines orogen hinge (Fig. 1-C) that hosts the southernmost intra-basin highs of the Plain (i.e., San Colombano, Casalpusterlengo, Zorlesco). They represent the different surface geomorphic expressions of the San Colombano (SCS)

and Casalpusterlengo-Zorlesco (CZS) ramp folds of the buried Apennines front (Zuffetti et al., 2018a; Zuffetti and Bersezio, 2021) which were the target for slip rates calculation.

3. Method

We integrated already published surface and subsurface geological data to build a 3D subsurface geological model used as input for the decompaction and unfolding of the Quaternary unconformity-bounded stratigraphic units deformed by the studied thrusts. Successive steps of fault restoration allowed computation of the Quaternary slip rates of faults. The workflow is shown in Fig. 2. The 3D integrated subsurface geological model that incorporates the geometry and chronology of the geological constraints derived from maps, cross-sections, and existing 3D subsurface model used for the computation of Quaternary slip rates.

3.1. Surface Geology

The surface constraining data belong to the recent geological maps of the central-southern Po Plain at 1:10,000 scale (Zuffetti et al., 2018a; Zuffetti and Bersezio, 2021) of the selected study area (Fig. 3). They permitted to characterise and down-trace stratigraphic boundaries and tectonic structures for surface-borehole correlations. We made a physical correlation among high-resolution stratigraphic logs by yielding the hierarchy and continuity of the unconformable boundaries between stratigraphic units and the record of their facies variability (Supplementary Information, Fig. S1). The work by Zuffetti and Bersezio (2021) provided a collection of age constraints of the Quaternary stratigraphic units and their bounding unconformities based on Optically Stimulated Luminescence (OSL) and ^{14}C age determinations. This information was used to constrain the shallow part of the geological sections used for the restoration (Fig. 4-A, B).

3.2. Subsurface Geology and integrated 3D geological model

The shallow subsurface dataset was presented in Zuffetti and Bersezio (2021). It comprised >500 subsurface log data: 252 water wells (max investigation depth around 200 m b.g.s.), 201 boreholes with core recovery, 46 geophysical soundings (max depth 300 m b.g.s.; Mele et al., 2018, Mele et al., 2014). All the logs were normalised, classified, and correlated along a 3D fence; in Fig. 3-B, the only ones intersecting the cross sections selected for this work are shown. The details of the Quaternary tectonostratigraphic framework of the San Colombano hill are schematised in Fig. 3-C.

The deeper structure relies on a comprehensive subsurface geological 3D model covering the entire Po Plain (D'Ambrogi et al., 2023, Fig. 3-D) as the result of the interpretation and integration of a whole set of 1338 2D seismic lines, 475 hydrocarbon wells (15 hydrocarbon wells publicly available on the ViDEPI database, www.videpi.com), and

constraints from surface geology.

The workflow adopted for the 3D model production included a first step of interpretation of the whole set of data and the interpolation (triangle-based tessellation) of the surfaces, both stratigraphic horizons and faults in the time domain (TWT). The second step was the analysis of 81 depth-time tables to create a 3D velocity model, and the time-depth conversion was performed with the Vel-IO 3D tool (Maesano and D'Ambrogi, 2017). Refining the 3D model in the depth domain included checking and adjusting geometric inconsistencies with independent constraints. According to the available data and the adopted modelling workflow, the faults and stratigraphic horizons resulted in surfaces fully describing their geometry (depth and dip) and relationships.

Within the study area, this model includes the surfaces of six main thrusts (F1A, F2aA, F2B, F3, F3a and F4 in this study) and two stratigraphic boundaries (i.e., Pliocene unconformity and Marine Quaternary unconformity, respectively ZU and GU in this study) based on the original interpretation of 44 seismic lines (Fig. 4) and 11 hydrocarbon wells (Fig. 1, ViDEPI; Eni SpA, non-exclusively confidential agreement, max depth 3000 m b.g.s.).

The publicly available seismic reflection profile "Appennino Centrale 1" of the ViDEPI database was integrated into the dataset (Fig. 4-C see Supplementary Information for details, Fig. S2). The seismic profile (Fig. 4-C) was converted from raster to SEG-Y using the tool Wiggle2Segy (Sopher, 2018) with an approach already tested for similar publicly available industrial seismic reflection profiles in the Italian region (Buttinelli et al., 2022).

The dataset's different origins, scales, and purposes forced us to address and resolve some discrepancies to obtain a single harmonised subsurface 3D model (Fig. 3-D). Notably, according to its geometry and diachronism across the whole basin, we considered the unconformity named Marine Quaternary in D'Ambrogi et al. (2023) comparable with the Gelasian Unconformity of this study. The constraints deriving from detailed surface analysis also imposed some modifications around San Colombano hill. Furthermore, where not modelled in the original 3D reconstruction due to the lack of data, we integrated the Pliocene unconformity from D'Ambrogi et al. (2023) with the geometry of Zanclean Unconformity from Fantoni and Franciosi (2010).

The geometry of sedimentary units, the relative chronology, and the timing of the geological evolution were composed in a hierarchic framework following the approach by Zuffetti et al. (2020). The architectural framework and the chronology of the target horizons benefit from the constraints provided by the existing regional literature data (geological boundaries and ages, Fig. 5).

We stored the comprehensive dataset of subsurface geological information in Move software (Midland Valley Exploration Ltd.). We used it to build a 3D integrated subsurface model of the target geological boundaries in this area. These were: i) five high-rank stratigraphic unconformities framing Calabrian to Late Pleistocene units (ZU, GU, U1, U2, U3) and ii) eight thrust surfaces. We selected the individual
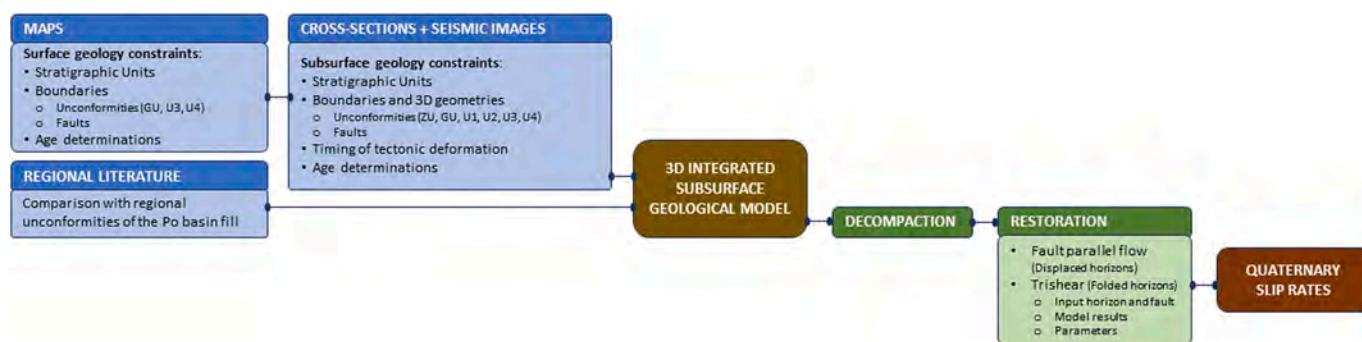

Fig. 2. The workflow proposed in the present work. It combines surface and subsurface geological data analysis and interpretation with quantitative modelling to decompact and restore the cross-sections and derive the slip rate values. ZU: Zanclean Unconformity, GU: Gelasian Unconformity, U1: intra-Calabrian Unconformity, U2: Lower-Middle Pleistocene Unconformity, U3: Middle-Late Pleistocene Unconformity, U4: Latest Pleistocene-Holocene Unconformity.
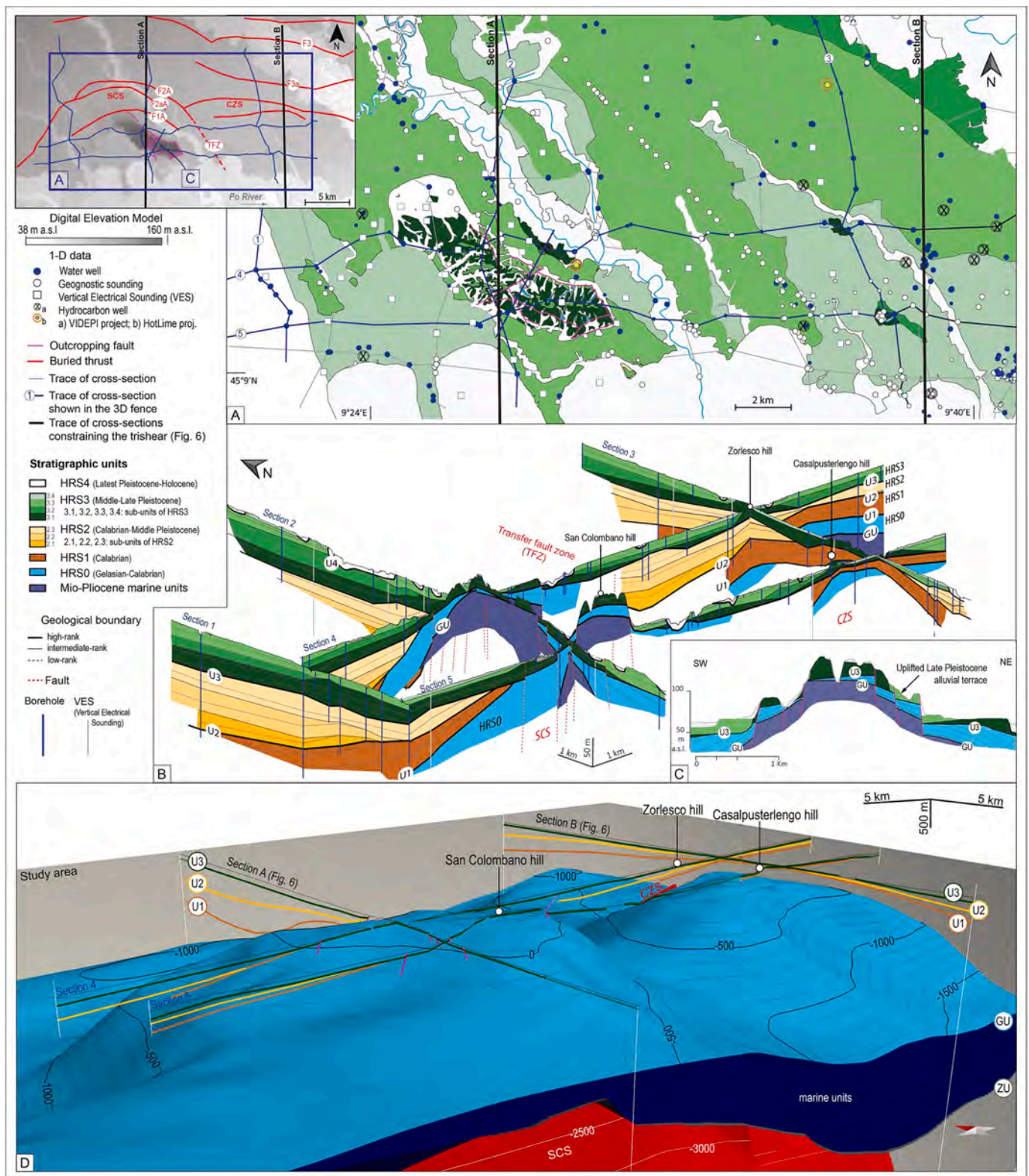
Fig. 3. The geological dataset. A) Geological map of the study area and B) shallow geological sections built from the geological map and borehole data (max depth: 200 m b.g.s). modified after Zuffetti and Bersezio (2021). C) Detail of the Quaternary tectonostratigraphic framework of the San Colombano hill along a SW-NE oriented cross-section, modified after Zuffetti et al. (2018). Within the five high-rank stratigraphic units HRS2 and HRS3, the colour scales highlight the component intermediate-rank stratigraphic sub-units. Details of the Quaternary tectonostratigraphy of Sections 2 and 3 in Fig. 4. D) 3D subsurface geological model derived from the interpretation of seismic reflection profiles (D'Ambrogi et al., 2023) and the integration of shallow geological sections (Zuffetti and Bersezio, 2021). Sections A and B, shown in Fig. 6, are used for the decompaction and restoration.
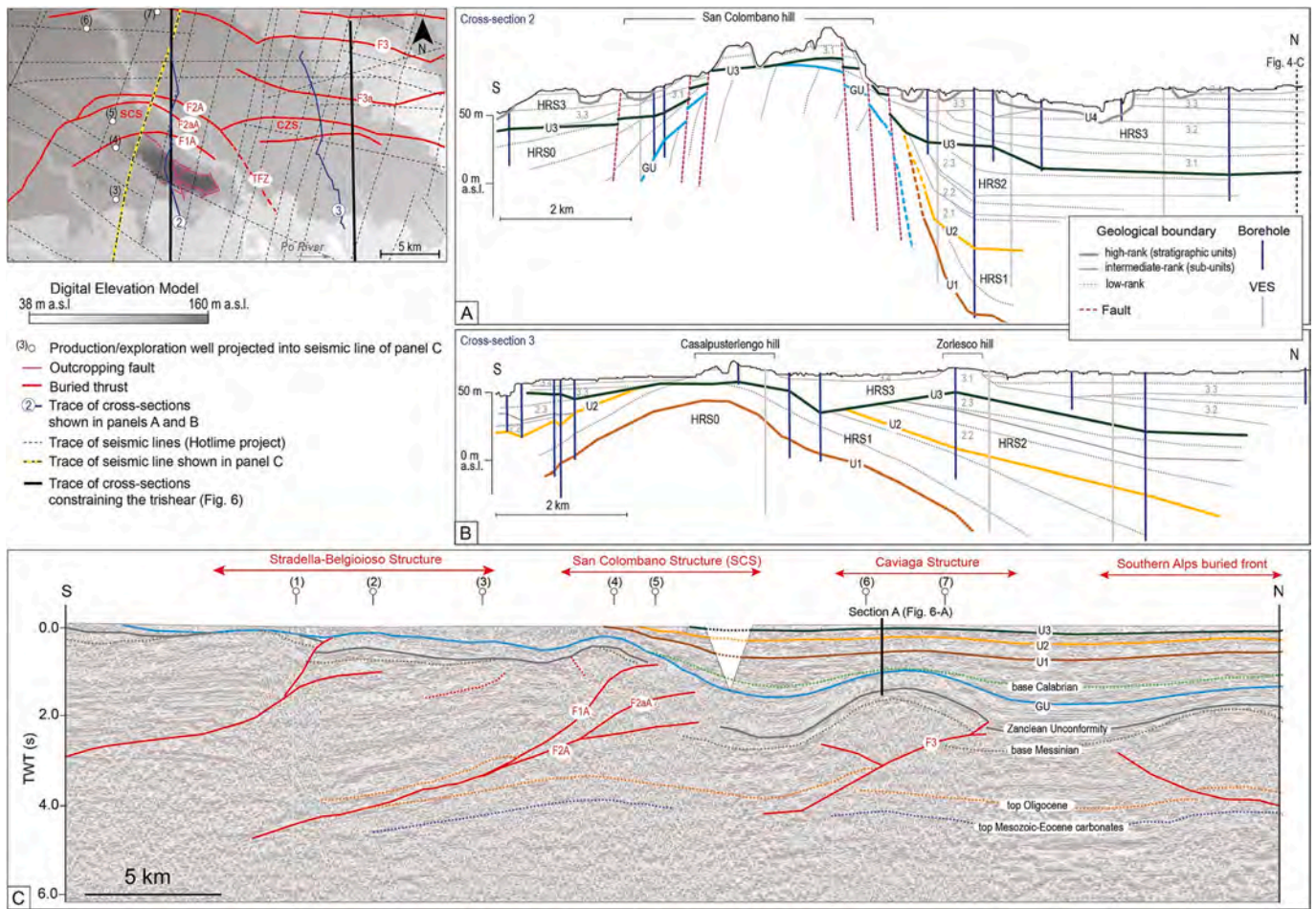
Fig. 4. A) Shallow stratigraphic section 2 crossing the San Colombano hill and parallel to the integrated Section A constraining trishear (Fig. 6-A). B) Shallow stratigraphic section 3 crossing the Casalpusterlengo and Zorlesco hills and nearly parallel to the integrated Section B constraining trishear (Fig. 6-B). The upper left box shows the position of seismic lines used by D'Ambrogi et al. (2023) for constructing the subsurface geological 3D (performed in the frame of HotLime Project). C) Interpreted seismic lines (App-Centr-1 line from ViDEPI, uninterpreted version in Supplementary information, Fig. S3) showing primary horizons and faults in the study area. Numbers refer to production/exploration wells. SCS: San Colombano Structure; CZS: Casalpusterlengo-Zorlesco Structure.

structures that were suited for an in-depth study of their tectonic evolution thanks to the completeness of the dataset and after comparisons with regional sections (Bigi et al., 1992; Fantoni and Franciosi, 2010; Pieri and Groppi, 1981).

Two cross-sections, running across SCS and CZS (sections A and B, respectively; Fig. 6), were extracted from the area's 3D integrated subsurface geological model. We chose the two sections' location and orientation to better describe the architecture and deformation history of the two tectonic structures.

3.3. Decompaction, restoration, and slip-rates calculation

The integrated cross-sections (Fig. 6) obtained in the previous step constituted the successive decompaction and restoration reference data. The amount of slip on the fault obtained at each stage allows for computing the differential slip rate associated with the faults during the corresponding deformation time. The decompaction allows for recovering the volume loss due to sedimentary loading and relative porosity reduction. The compaction effect is higher in the syncline succession and less pronounced in the anticline; thus, the decompaction procedure is necessary to avoid the overestimation of fold amplitude (Amorosi et al., 2021). This overestimation would eventually affect the calculation of the fault slip estimation and, consequently, the slip rates. The previous estimate of the impact of differential compaction on the assessment of tectonic deformation suggests that the fold amplitude of growth strata

across thrusts will reduce up to 30–40% after decompaction (Maesano et al., 2015), the offset measured across normal faults may reduce of 15% (Taylor et al., 2008), and strain rate across thrusts may reduce of up to 30% (Pizzi et al., 2020). Once we remove the load associated with a layer of sediments, the eventual residual deformation of the underlying levels can be related to tectonic deformation (Maesano et al., 2015; Panara et al., 2021).

The porosity reduction of a sedimentary layer with its progressive burial generally follows an exponential function (Allen and Allen, 2013). Various parameters for this relationship have been proposed based on different lithologies, burial depths, and time. In this work, we applied the equation proposed by Johnson et al. (2018) for the recent most mainly sandy continental deposits that have experienced <500 m of burial:

$$\Phi = -0.0315 ln(s) - 0.0350 ln(z) + 0.7385$$

where φ is the porosity at a given depth (z) as a function of the grain size (s). We modelled the deeper horizons following the classical equation of Sclater and Christie (1980), assuming a composition made by an equal mixture of shale and sand (Maesano et al., 2015; Maesano et al., 2013; Panara et al., 2021; Scrocca et al., 2007).

After each decompaction step, we progressively restored the residual deformation observed on each horizon. The restoration allows the calculation of the slip along the underlying fault necessary to unfold the selected stratigraphic horizons to their original depositional geometry.
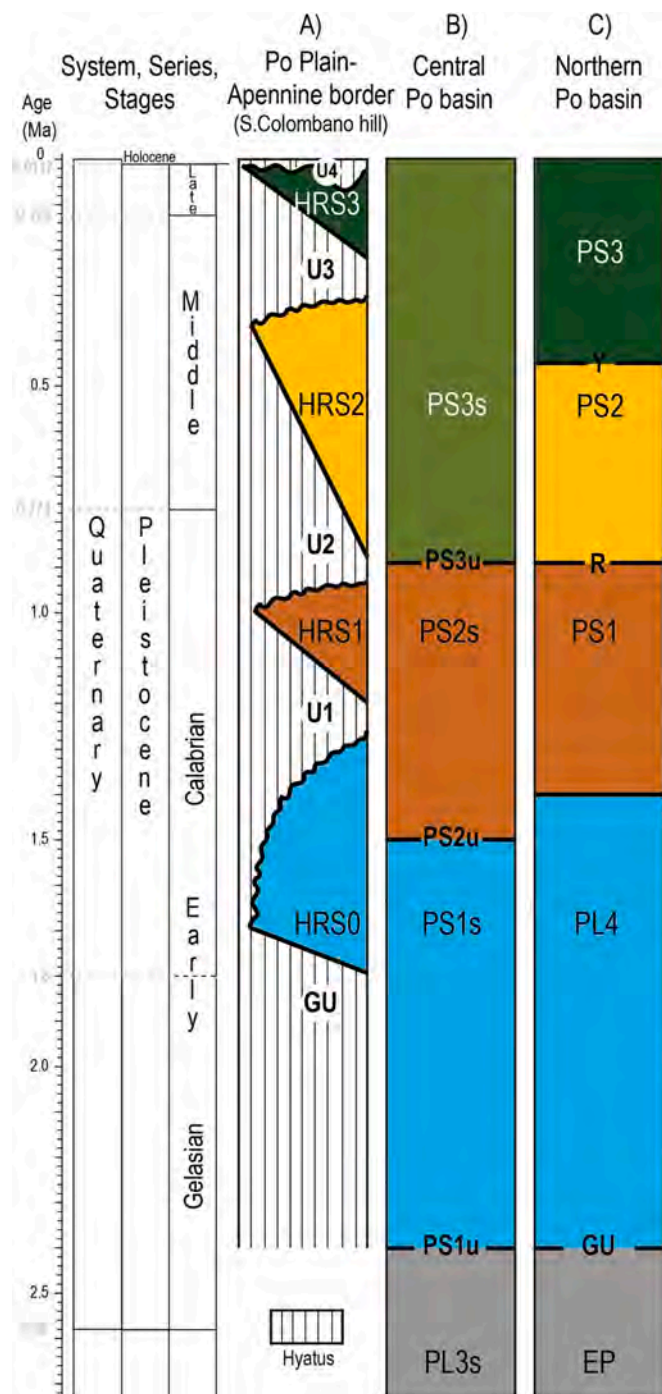
Fig. 5. Chronostratigraphic scheme of the Plio-Quaternary fill of the Po basin. Column A: the target unconformities of this work at the southern margin of the basin at the Po Plain-Apennines border, modified after Zuffetti and Bersezio, 2021. These boundaries are compared with the stratigraphy of the basin fill proposed in the literature: Column B) after Amadori et al., 2019; Column C) after Ghielmi et al., 2013, 2010; Scardia et al., 2012. Chronostratigraphic correlation table after Cohen and Gibbard (2019).

Among the various kinematic methods commonly used to restore geological structures appropriately, we adopted the trishear algorithm (Allmendinger, 1998; Erslev, 1991). The trishear approach allows for restoring the folding ahead of the fault tip and is suitable for studying complex fault propagation folds (Allmendinger et al., 2011). Among the various kinematic approaches to studying thrust-related folds, trishear also proved to be effective in reproducing the fold with realistic

geometries and rates of deformation (Gold et al., 2006) and is thus reliable for the successive slip rate calculation. In trishear modelling, the fold geometry depends on the shape of a triangular shear zone emanating from the fault's upper tip. The parameters controlling the modelling are the fault tip location (x, y), the amount of slip, the fault ramp dip (ra), the angle of the trishear zone (ta), and the ratio between the fault propagation and the slip (p/s). The inverse trishear modelling requires minimising the difference between modelled and observed fold geometry by varying all the parameters involved in the trishear formulation. Given the number of variables involved in the restoration, the solution is not univocal (Cardozo et al., 2011; Oakley and Fisher, 2015).

In this study, we used the trishear formulation proposed by Cardozo et al. (2011) and modified after Panara et al. (2021) to consider the prior knowledge of the fault geometry in weighing the solutions. Cardozo et al. (2011) solve the inverse trishear through the simulated annealing optimisation method. Instead of systematically testing the parameter space, simulated annealing is a stochastic procedure that provides the best-fit model as the combination of parameters that globally minimises the least squares linear regression error of the restored horizons.

We performed five independent runs of 10,000 inversions for each structure and each horizon. In cases of multiple splays at the tip of a master fault, we considered a single fault with the average parameter of the master fault. We limited the parameter space search for the variables where the prior geological knowledge provides strong constraints. Specifically, we searched for the fault tip coordinates (x, y) in the area bounded by the lower and upper coordinates of the fault ramp in the geological cross sections. The search space for the fault dip was limited to $\pm 5°$ around the fault dip value measured in the cross-sections. We set up a broader space search for all the other parameters: 20–80° for the trishear angle (ta) and 0–3 for the ratio between propagation and slip (p/s). We performed a preliminary inversion run with a search space between 0 and 2 km for the slip parameter and then made a second refined run using a narrower search window for each case. The trishear inversion places the solutions within a rectangular area limited by the fault's coordinates. The inversion solutions have different weights based on the distances from the fault trace and the inversion residual (Panara et al., 2021). The inversion solutions with the highest weight are closer to the fault trace and have smaller residuals from the inversion. The weight decreases linearly with the increasing distance from the fault and for higher residual of the solutions. We normalised the weight associated with each inversion to make the results comparable between the various faults and horizons.

In the case of faulted horizons, where we could directly estimate the displacement from the cut-off, we used the Fault Parallel Flow method (Egan et al., 1999) to restore the on-fault deformation. We summed the displacement to the slip computed with the trishear. The slip's variability (standard deviation) in the trishear solutions and the uncertainty in estimating the horizons' age is the input data for the slip-rate assessment.

We computed the probabilistic slip rates according to the approach proposed by Zechar and Frankel (2009), modified to take into consideration the case of not-null probability of negative slip in the tail of the Gaussian curve. We considered the age brackets and uncertainties on the restoration of the horizons bounding the stratigraphic units. We used a probabilistic density function (PDF) with a boxcar shape, assuming a not-null probability only in the time interval between the horizons' age uncertainties. The combination of the Gaussian PDF of slip and boxcar PDF of time interval allows for computing the PDF of the slip rates (Zechar and Frankel, 2009).

4. Geological constraints for slip-rates computation

The Quaternary southern Po basin fill of the study area comprises five stratigraphic units (HRS0 to HRS4; Fig. 3; Table 1; Fig. 4) bounded by unconformities of high hierarchic rank: Gelasian Unconformity (horizon GU), intra-Calabrian unconformity (U1), Early-Middle Pleistocene
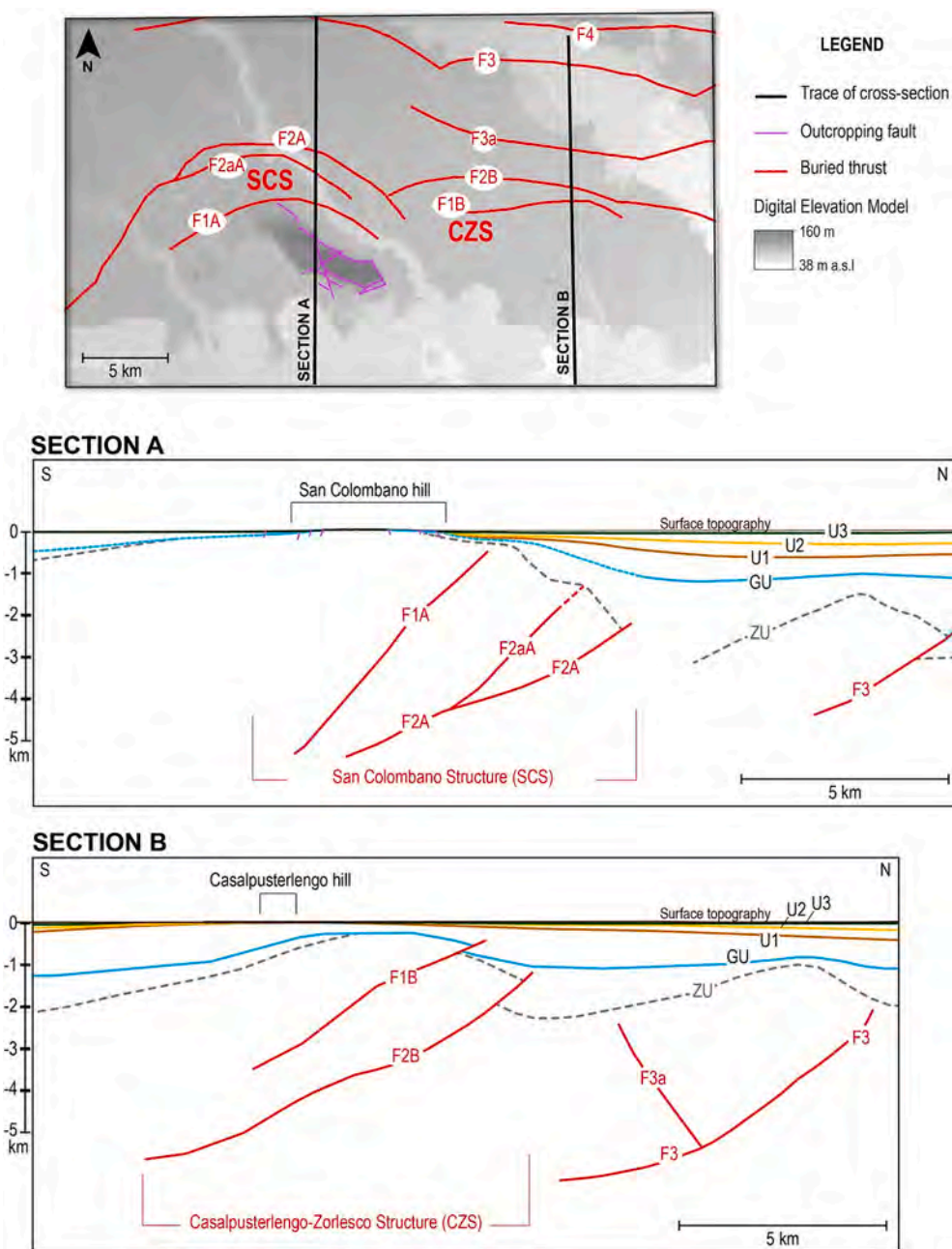
Fig. 6. Integrated geological model constraining the trishear. Above: structural map and Digital Elevation Model of the central southern Po Plain. Buried thrust traces after Bigi et al. (1992); D'Ambrogi et al. (2023); Rossi et al. (2015); outcropping faults after Zuffetti et al. (2018a). Below: selected cross-sections extracted from the integrated 3D subsurface geological model. A: N-S oriented section across the San Colombano Structure (SCS). B: N-S oriented Section across the Casalpusterlengo-Zorlesco Structure (CZS). Map on top refers to the study area (inset Fig. 1C). Labelling of stratigraphic boundaries in Fig. 5. F1A, F2A, F2aA are thrust faults of the SCS; F1B and F2B are thrust faults of CZS, F3 and F3a are thrust faults of the Caviaga-Soresina structure (see Figs. 1 and 4).

Table 1
Age constraints to the stratigraphic boundaries defined in this work and used as chronological constraints for slip rate calculation. The age estimates (Ma) report the older and younger values for the base and the top of each stratigraphic unit. The maximum and minimum possible interval duration is used as a boxcar distribution in the slip rates computation. The duration variability is computed as the maximum less minimum interval duration.

Unit	Min-max thickness (m)	Horizon Base	Horizon Top	Age base (Ma)	Age top (Ma)	Min interval duration (Ma)	Max interval duration (Ma)
HRS3	5–80	U3	U4	0.28–0.13	0.01–0	0.12	0.28
HRS2	40–120	U2	U3	0.95–0.86	0.28–0.13	0.58	0.82
HRS1	0–150	U1	U2	1.24–1.14	0.95–0.86	0.20	0.39
HRS0	5–90	GU	U1	2.40–1.80	1.24–1.14	0.56	1.26

unconformity (U2), Middle-Late Pleistocene unconformity (U3) and Latest Pleistocene-Holocene unconformity (U4). A detailed description of sedimentary features, architecture, and incremental geological evolution of these units is reported by Zuffetti and Bersezio (2021), relying on surface and shallow subsurface datasets along a grid of stratigraphic cross-sections (Fig. 3-A, B, C). Thanks to the integration with the 3D geological model derived from the interpretation of reflection seismic profiles (Fig. 3-D) in the study area and relying on the available age constraints, we used the 3D architectural and chronological framework of the targeted Quaternary geological boundaries as input for the trishear. Age constraints to the computation derive from the definition of older and younger ages for both the bottom and top of each high-rank stratigraphic unit in the study area. The resulting age range of the target unconformable boundaries (Table 1) was compared with the chronostratigraphic attributes of the correlative horizons in the depocentral regions of the central Po basin available in the literature (Fig. 5). In the following sections, the essential features of the stratigraphic boundaries and units and the features of the target structural boundaries, are summarised.

4.1. Stratigraphic boundaries

4.1.1. Horizon GU: gelasian unconformity

GU bounds an Early Pleistocene clayey marine succession punctuated by transgressive-regressive cycles (HRS0; Fig. 3-B, Fig. 4, Fig. 5) developed after Gelasian uplift along the San Colombano and Casalpusterlengo-Zorlesco structures (Zuffetti and Bersezio, 2021). GU crops out in the San Colombano hill, gently folded by an ENE-WSW-trending anticline. In contrast, GU is buried at the Casalpusterlengo and Zorlesco hills (Fig. 3-B, Fig. 4-B) and is folded along a WNW-ESE-trending gentle anticline. GU cuts down to the Miocene formations at the crest of these folds. According to the 3D model derived from seismic lines interpretation (D'Ambrogi et al., 2023; Fig. 4-C), the anticline folding closes east of Casalpusterlengo and Zorlesco hills, plunging toward SE. In the back limb, south of these hills, a syncline deepens up to 1200 m, controlled by the thrusts shaping the outer Emilia Arc.

GU started to develop before the first occurrence of *Hyalinea Balthica* and *Arctica Islandica* (early age in the Arda and Stirone sections is around 1.8 Ma; Table 1), predating the first occurrence of *Truncorotalia truncatulinoides excelsa* (Zuffetti and Bersezio, 2021) within the overlaying HRS0. Deposition of this unit lasted up to the lower part of the *G. Cariacoensis* zone and ended around the end of the "Early-Middle Pleistocene transition" (Zuffetti and Bersezio, 2021). Regionally, HRS0 corresponds to part of the generic "Marine Quaternary" defined in logs from the hydrocarbon wells drilled in the central Po Plain (e.g., Secugnago 02, Casalpusterlengo 5, data available on ViDEPI). The age attributions to the correlative boundaries in the Central Po Plain (Gelasian Unconformity; PS1 horizon; Fig. 5; Amadori et al., 2019; Ghielmi et al., 2013, Ghielmi et al., 2010; ISPRA, 2015) allow inferring an older age of GU of 2.4 Ma.

4.1.2. Horizon U1: Intra-Calabrian Unconformity

U1 bounds an overall regressive clayey-sandy sequence from lagoonal to deltaic, up to alluvial environments (HRS1; Fig. 3- B, Fig. 4) that might correspond to the eastward progradation of the Po basin trunk river and its tributaries during the Calabrian (Zuffetti and Bersezio, 2021). U1 dips away from the crest of the San Colombano structure and Casalpusterlengo-Zorlesco fold (Fig. 3 and Fig. 4).

HRS1 sediments postdate the first occurrence of *H. balthica* and *A. islandica* and the end of *G. Cariacoensis* zone (1.14 Ma; Crippa et al., 2018) and do not contain the Middle Pleistocene microfaunal associations (Bini et al., 2016). Hence, its deposition was constrained to the Calabrian, likely beginning at the "Early-Middle Pleistocene transition" matched to MIS36 (around 1.24 Ma; Cohen and Gibbard, 2019). Relying on these constraints the unconformity U1 postdates the intra-Calabrian unconformity (Ghielmi et al., 2013; Scardia et al., 2012; Fig. 5- column

C) and the horizon PS2u (Fig. 5-column B; Amadori et al., 2019) in the central-eastern Po basin, and may be compared either to QM2 or to QM3 of ISPRA (2015).

4.1.3. Horizon U2: Early–Middle Pleistocene Unconformity

U2 bounds the first Pleistocene large-scale continental regressive trend associated with uplift and folding along the San Colombano and Casalpusterlengo-Zorlesco structures (Zuffetti and Bersezio, 2021). U2 dips away from the hinges of the km-scale San Colombano and Casalpusterlengo-Zorlesco anticlines, Fig. 3; Fig. 4. This unconformity bounds the alluvial sedimentary units composing HRS2, which are missing below U3 in the San Colombano and Casalpusterlengo hills and the southernmost study area. Older ages of U2 correlate with the onset of the Calabrian advance of South Alpine glacial amphitheatres (Bini et al., 2016), ranging between 0.95 (estimated onset of MIS 22) and 0.86 Ma (estimated onset of major Pleistocene glaciations in the Alps; Muttoni et al., 2003; Table 1, Fig. 5). U2 dates up to 0.28 Ma, as constrained by the infrequent occurrence of *Carya* and *Pterocarya* pollens that spread from the upper Middle Pleistocene (Moore et al., 1991; Zuffetti and Bersezio, 2021). Relying on age interval and stratigraphic position of U2, HRS2 comprises PS2 and part of PS3 sequences of Scardia et al. (2012), compares with PLCa-b units of (ISPRA, 2015) in the central Po basin; it overlaps part of PS1 and PS2 of Ghielmi et al. (2013) and the lower part of PS3s of Amadori et al. (2019) (Fig. 5).

4.1.4. Horizon U3: Middle-Late Pleistocene Unconformity

The U3 angular unconformity results from the Middle-Late Pleistocene interaction between glacial-fluvial deposition and contemporaneous uplift, wrenching, and collapse at the San Colombano and Casalpusterlengo-Zorlesco structures. This evolution determined the development and displacement of intermediate-rank alluvial terraces composing unit HRS3 above and around the two anticlines (Fig. 3-C; Fig. 4-A, Fig. 4-B). U3 and HRS3 get gently folded and offset by extensional faults at the San Colombano hill (Fig. 3-C and Fig. 4).

The age of the progressive unconformity U3 (Table 1) is based on radiocarbon and OSL age determinations on both surface and subsurface samples of HRS3 and its cross-cut relationships with the underlying units (Zuffetti and Bersezio, 2021). In the study area, the oldest ages of U3 relate to the advance of the Middle Pleistocene alpine Verbano and Lario glacial amphitheatres (Bini et al., 2016), ranging between 0.28 Ma (estimated onset of MIS 8; Table 1, Fig. 5) and 0.13 Ma (estimated onset of Marine Isotopic Stage MIS6). U3 likely developed up to 0.013 Ma (end of the Last Glacial Maximum) before the development of the Latest Pleistocene-Holocene unconformity U4, owing to the entrenchment of the river network. U3 postdates the unconformities Y (Scardia et al., 2012) and QC3 (ISPRA, 2015) correlated in the central Po basin. HRS3 might correspond to either the upper part of PS3 (Scardia et al., 2012; Fig. 5-column C) or PLCc (ISPRA, 2015) or to the upper part of PS2 (Ghielmi et al., 2013) or PS3s (Amadori et al., 2019) (Fig. 5-column B).

4.1.5. Horizon U4: Latest Pleistocene-Holocene Unconformity

U4 bounds the lowermost alluvial terraces entrenched within the main morphological surface of the Po Plain and includes the deposits of the present-day river network (HRS4; Fig. 3). Relying on radiocarbon age determinations, the age of U4 ranges between ca. 0.013 and 0 Ma since U4 is still under formation (Zuffetti and Bersezio, 2021).

4.2. Tectonic boundaries

The structures SCS and CZS represent two anticlines controlled by two thrust systems, detached on the Oligocene units, that shaped the western portion of the Outer Emilia Arc (Fig. 1): the San Colombano Thrust System represents the ramp of the arc, with a strike from *E*-W to NNE-SSW, moving westward, on the other hands the Casalpusterlengo-Zorlesco Thrust System is mainly E-W trending in the study area, with a strike changing to NW-SE moving eastward. The 3D geometries of the

faults of these thrust systems are derived from Fantoni and Franciosi (2010) and D'Ambrogi et al. (2023).

4.2.1. San Colombano Thrust System

The San Colombano Thrust System includes at least three thrusts in the studied area (Fig. 4-C; Fig. 6 sect. A). The northern and outer thrust (F2A) displaced the Pliocene unconformity (Zanclean Unconformity, ZU) and deformed the younger horizons. This thrust is replaced eastward, between San Colombano and Casalpusterlengo, by the main thrust of the Casalpusterlengo-Zorlesco Thrust System (F2B) that evolved together during Miocene and Pliocene. F2A splays out in two thrusts moving up dip; in Fig. 6, we maintain the nomenclature of the main thrust (F2A) for the deeper splay and named the shallower one F2aA. Both splays contributed to the deformation of the Pliocene and younger unconformities. A steeper dip characterises the innermost thrust of the system (F1A) compared to F2A (Fig. 4 and Fig. 6). The whole thrust system is responsible for the uplift of the San Colombano hill.

4.2.2. Casalpusterlengo-Zorlesco Thrust System

The Casalpusterlengo-Zorlesco Thrust System (Fig. 6, sect. B) is a W-E-oriented structure with a main thrust (F2B) displacing the Pliocene unconformity (ZU). It is responsible for the deformation of GU and the uplift of the Casalpusterlengo and Zorlesco subtle reliefs. A minor and younger thrust (F1B) developed in the hanging wall of F2B, cutting its forelimb and displacing GU.

5. Results of restoration

The restoration of the deformation observed in the two cross-sections is related to the effect of tectonic displacement and differential compaction of growth strata. To assess the impact of the differential compaction, we performed six different synthetic forward models in which we completely controlled all the trishear tectonic displacements. Then, we restored the same sections after applying the sediment compaction (Supplementary Information Fig. S4). The results of the synthetic tests suggest that not considering the differential compaction may lead to an overestimation of the tectonic displacement of 30–45%, depending primarily on the lithologies involved in the compaction process (Supplementary Information, Table S1).

We performed the systematic procedure of decompaction and restoration to recover the deformation produced by Fault F1 and Fault F2 in the two cross-sections of Fig. 6. The process started from the younger stratigraphic horizon and proceeded toward the older ones. We restored the gentle folding deformation that affected the shallower horizons (U3, U2 and U1) using the trishear method. The deeper horizon for which we made our calculation (GU), instead, is characterised at places by some offset along the fault F1B (Fig. 6, sect. B); in this case, we recovered the offset by using the Fault Parallel Flow method, and we restored the remaining folding using the trishear. For each restoration step, we selected the segment of each horizon located ahead of the fault tip and computed the trishear inversion. The following describes a representative example of the inversion outcome (Fig. 7) performed on
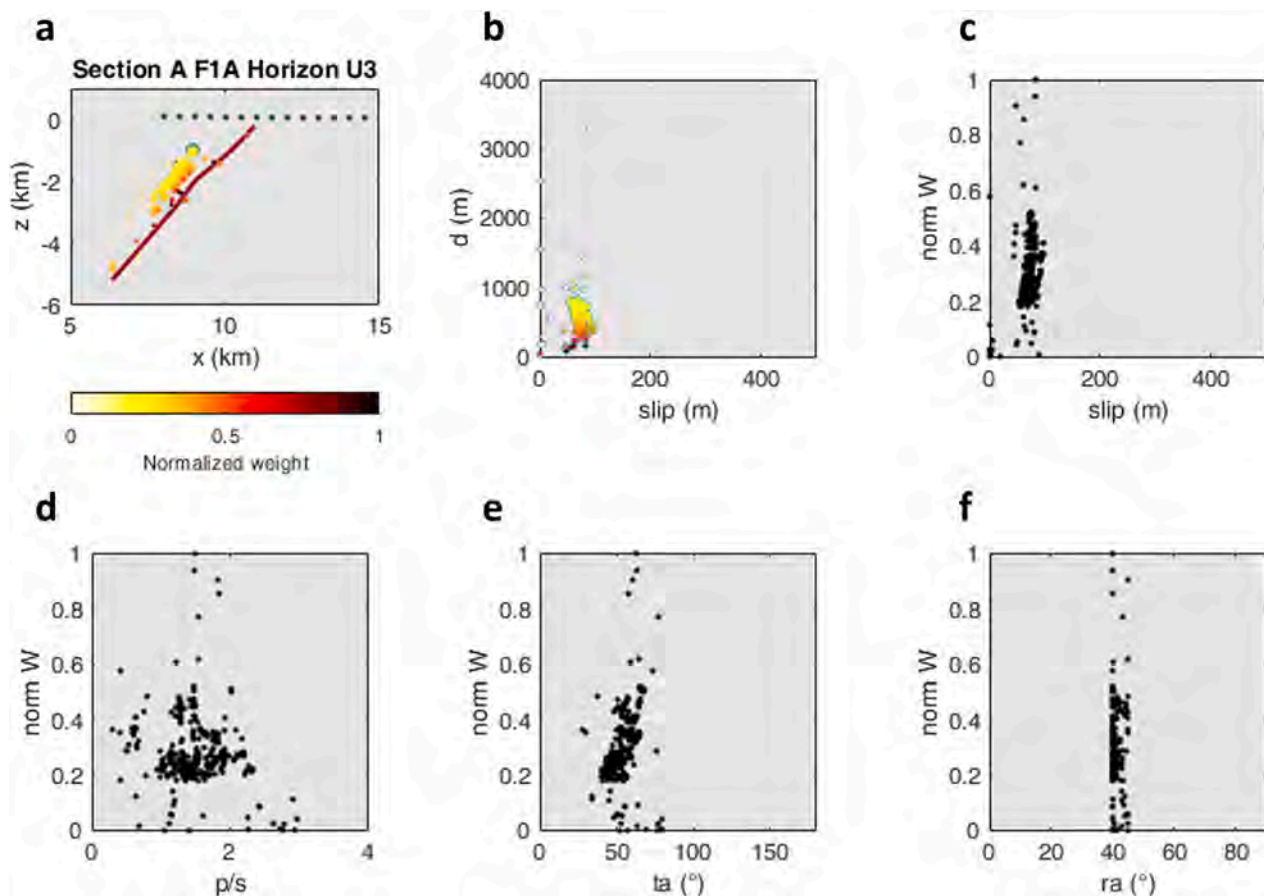

Fig. 7. Example of trishear inversion for the horizon U3 on section A. a) schematic section of trishear inversion; brown dots represent the U3 horizon, dark red line represents the fault F1A (Fig. 6), gradient scale dots represent the tip position of the inverted faults, colour gradient represent the normalised weight defined as (1-fval)*(1/d) where fval is the normalised value of the regression function (Cardozo et al., 2011; Panara et al., 2021); b) distribution of the inverted fault model for slip value and distance from the fault F1A mapped in Section A (Fig. 6), colour gradient represents the normalised weight; c) distribution of the inverted fault for slip and normalised weight; d) distribution of the propagation vs slip (p/s) for the fault inversion; e) distribution of trishear angle (ta) for the fault inversion; f) distribution of ramp angle (ra) for the fault inversion. (For interpretation of the references to colour in this figure legend, the reader is referred to the web version of this article.)

Table 2

Summary of the results of the trishear inversion. Slip: weighted average slip of the inversion. Slip_dev: standard deviation of slip from the inversion. FPF: slip value restored with Fault Parallel Flow; ra: weighted average ramp angle from inversion; ra_dev: standard deviation on ramp angle; ta: weighted average trishear angle from inversion; ta_dev: standard deviation on trishear angle; p/s: weighted average propagation vs slip ratio from the inversion; p/s_dev: standard deviation on p/s.

Section A										
Fault	Horizon	Slip trishear (m)	Slip dev (m)	FPF (m)	ra (°)	ra dev (°)	ta (°)	ta dev (°)	ps	ps dev	Note
F1A	U3	71	10	–	41.2	0.47	53.7	6.75	1.46	0.34	cumulative F1A and F2A
	U2	114	35		43.2	3.6	45.8	21.17	1.88	0.82	
	U1	47	12	–	42.5	2.42	55.6	15.79	1.26	0.299	
	GU	–	–	–	–	–	–	–	–	–	
F2A	U3	–	–	–	–	–	–	–	–	–	
	U2	316	74		23.3	2.95	50.3	10.25	1.8	0.45	
	U1	291	28		28	0.23	64.1	13.14	2.2	0.59	
	GU	665	82	–	29.6	1.78	47.8	26.19	0.98	0.44	cumulative F1A and F2A

Section B										
Fault	Horizon	Slip trishear (m)	Slip dev (m)	FPF (m)	ra (°)	ra dev (°)	ta (°)	ta dev (°)	ps	ps dev	Note
F1B	U3	–	–	–	–	–	–	–	–	–	
	U2	38	6		28.4	2.46	58.1	10.94	1.56	0.57	
	U1	52	29	–	27	2.32	60.5	11.58	1.73	0.67	
	GU	276	12	363	37.9	2.11	27.5	7.24	1.996	0.698	
F2B	U3	42	24	–	25.4	4.66	55.7	12.59	2.16	0.79	cumulative F1B and F2B
	U2	56	23	–	26.4	1.83	60.8	7.99	1.34	0.41	
	U1	66	13	–	26.9	1.93	70.2	12.02	1.73	0.75	
	GU	370	44	–	26.7	2.85	73.6	5.14	1.75	0.71	

horizon U3. The Methods section provides the meaning of the trishear parameters. Table 2 synthesised the results of all the inversions for all the horizons, whereas the Supplementary Materials (Fig. S5-S17) include all the details of the inversions.

In the trishear inversion example of Fig. 7, it is possible to notice that a large part of the tested points in the inversion is close to the fault trace, suggesting that the folding of the selected horizon is well explained by the fault traced in the cross-section. The slip values and trishear angle (ta) show a strongly picked distribution, whereas the propagation vs slip ratio (p/s) has a more dispersed distribution. The sharp distribution of slip values indicates that the inversion is stable for most of the tested solutions, reflected in the standard deviation value reported in Table 2. The limited variability in the trishear angle (ta) indicates that the geometry of the fold can be fitted within a narrow range of possible trishear zones. In contrast, the variability of p/s ratio indicates that various solutions of fault propagation during fault slip may fit the observed deformation. This observation is relevant especially for low slip values, since the fault propagation may vary significantly without significantly affecting the fold geometry.

The slip required for unfolding the horizons in the two cross-sections shows a general decreasing trend during the Quaternary, ranging from several hundred meters for GU to a few tens of meters for U3 (Table 2). Some deviations from this trend are observed in Section A and will be discussed in the following.

In the case of Section A (San Colombano Structure), we observed that fault F1A allows for better recovery of the deformation of U3; however, the very gentle folding and the distance from the deep fault tip of F2A may influence these results, and thus, the final value represents a cumulative estimate for both the two structures. The activity of F1A started to control the geometry of the entire anticline after the deposition of unit HRS1. In contrast, fault F2A better explains the deformation of GU even if F1A may have contributed to the folding, and thus, the slip value is cumulative for both faults. Since GU is eroded in correspondence with the San Colombano hill, the slip value computed in the inversion for this horizon should be taken as a minimum. The deformation observed in the horizon U2 requires slightly higher slip values than what is needed to deform U1; this result may indicate a deformation pulse on the faults mapped in Section A recorded by U2. The secondary normal faults mapped in the axial part of the San Colombano anticline (Section A,

Fig. 6) are characterised by offset ranging between 2.5 and 30 m.

Section B (Casalpusterlengo-Zorlesco Structure) shows a very gentle deformation of U3, which, after the decompaction, becomes almost negligible. The inversion of this horizon can be achieved only by considering the cumulative effect of F1B and F2B. The older horizons show a decrease in the slip values during the Quaternary. The values computed for horizon U2 should be considered minimum estimates due to erosion in the axial part of the anticline after deposition. The inner structure F1B shows a displacement of 363 m at GU, recovered with the Fault Parallel Flow method, and the residual folding was restored with the trishear method.

The cumulative Quaternary slip associated with both faults is slightly higher for Section A (ca. 1520 m versus 1260 for Section B). Still, it has a different distribution through time since the faults in Section B accumulated more slip than those in Section A before the origin of U2. Conversely, Section A's faults prevail over Section B's after U2.

6. Slip rates of the San Colombano and Casalpusterlengo-Zorlesco Structures

The combination of the constraints on the age of deformed horizons and the computation of slip required to justify the residual folding after decompaction allowed for computing the probabilistic distribution of the slip rates along the faults traced on the two cross-sections.

The time intervals along which the deformation occurred are represented with a boxcar distribution that includes both the time elapsed and the uncertainty on the upper and lower limit of the time interval. The combination with the slip values (described as a Gaussian function by the average value and the standard deviation) produces asymmetrical bell-shaped curves (Fig. 8) with short tails toward the lower values and longer tails toward higher values of slip rates.

The slip rates for the Calabrian to Late Pleistocene units (HRS1, HRS2 and HRS3) are higher for F1A and F2A in Section A (San Colombano Structure) compared to the faults in the same structural position in Section B (Casalpusterlengo-Zorlesco Structure; Table 3). Both the faults in Section B show a pronounced slowing of their activity after the deposition of HRS1.

We computed the cumulative slip rates for sections A and B (Fig. 8, Table 3; Fig. 9) by summing the slip values for all the faults associated
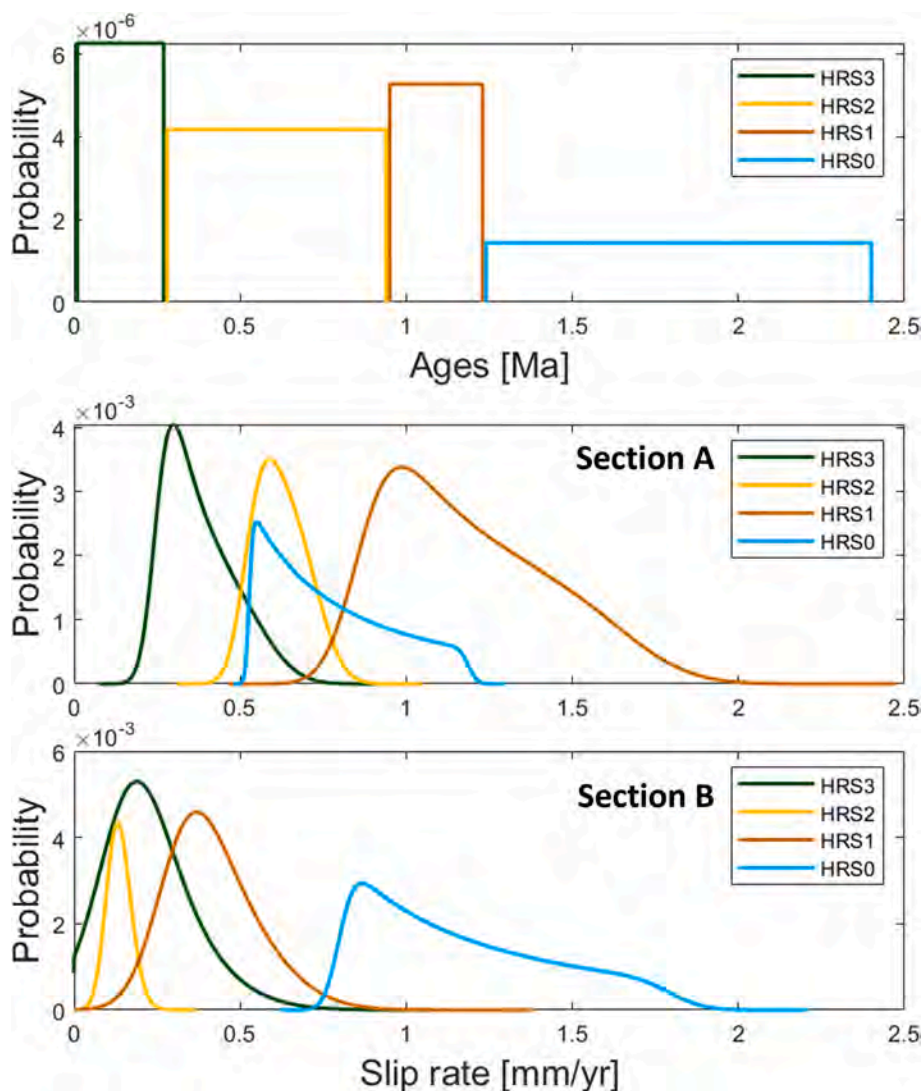
Fig. 8. Probability curves for cumulative slip rates obtained using a modified version of the code from Zechar and Frankel, (2009). Top panel: boxcar distribution of the time interval used for the slip rate calculation. Central panel: cumulative slip rates probability curve for section A across the San Colombano Structure (SCS). Notice that HRS0 has a mode for lower values than HRS1 and HRS2 due to the erosion of GU at the San Colombano relief and thus represents a minimum estimate. Bottom panel: cumulative slip rates probability curve for Section B across the Casalpusterlengo-Zorlesco Structure (CZS). Notice that HRS3 has a similar mode value to HRS2 but with a broader distribution showing a not-null probability for slip rates of 0 mm/yr.

with the two fault systems.

The comparison of the slip rate distributions clearly shows a general decrease in values for the more recent time intervals, marked by the shift of the probabilistic distribution toward lower values. Unit HRS0 in Section A represents a remarkable exception since the erosion truncated the GU horizon along the San Colombano hill. Thus, the measured slip rate must be considered as a minimum. The significant difference in the distribution between the two cross sections is that Section A (SCS) shows a distribution that falls to negligible probability for null slip rate values for HRS3; Section B, instead, indicates that the CZS has a truncation of the slip rate probability at 0 mm/yr for the same unit, which suggests that the likelihood of a slip rate equal to 0 is not null. This observation reflects the high uncertainty in the inversion of the deformation for Base U3 in section B (Table 3).

7. Discussion

The analysis and integration of data available for the frontal part of the Apennines Emilia Arc allowed for constraining the geometry and Quaternary kinematic evolution of the main buried faults recognised in

the area (Fig. 9).

The general structural setting of this portion of the Emilia Arc shows the presence of three main thrust systems controlling the development of the associated anticlines. From south to north, the recognised structures (intended as both the thrust system and the related anticlines) are the Stradella-Belgioioso structure, the San Colombano and Casalpusterlengo-Zorlesco structures, and the Caviaga-Soresina structure (Fig. 1, Fig. 4-C, Fig. 6). The latter represents the outermost Northern Apennines culmination that is facing the Southern Alps buried thrust front (Fig. 4-C). All the frontal thrusts detach within the Oligocene stratigraphic units (Fantoni and Franciosi, 2010; Pieri and Groppi, 1981) in their outer part (Fig. 4-C), and they possibly root at a deeper structural level in the innermost part of the chain of the Emilia Arc where they connect to a seismogenic segment in the lower crust (Tibaldi et al., 2023).

The results of this work provided a detailed reconstruction of the Quaternary slip history recorded by the main buried frontal thrust of the Emilia Arc. Previous estimates of slip rates in the study area came from the regional scale works of Boccaletti et al. (2011) and Maesano et al. (2015). Both these works provided slip rate values averaged over the last

Table 3

Summary of the slip rates computed for each fault belonging to SCS and CZS and cumulative estimate for the two anticlines for each time interval covered by the stratigraphic units (see Table 1). For the cumulative slip rate values, the uncertainty of the slip is computed as the quadratic error of the standard deviation for each fault reported in Table 2. The Mode represents the more frequent value of the distribution and is taken as a reference. P5, P13, P32, P68, P87 and P95 represent the slip rates value corresponding to the 5th, 13th, 32nd, 68th, 87th, and 95th percentile of the cumulative probability distribution.

Section A		Slip rates (mm/yr)									
Fault F1A	Unit	Mode	Average	Median	Standard dev	P5	P13	P32	P68	P87	P95
*	HRS3	0.30	0.38	0.54	0.27	0.12	0.20	0.37	0.71	0.89	0.96
	HRS2	0.16	0.16	0.21	0.17	0.00	0.00	0.11	0.32	0.42	0.47
	HRS1	0.15	0.17	0.25	0.16	0.00	0.04	0.15	0.35	0.46	0.51
	HRS0	–	–	–	–	–	–	–	–	–	–
Fault F2A	Unit	Mode	Average	Median	Standard dev	P5	P13	P32	P68	P87	P95
	HRS3	–	–	–	–	–	–	–	–	–	–
	HRS2	0.44	0.46	0.56	0.36	0.00	0.10	0.33	0.78	1.02	1.12
	HRS1	0.85	1.02	1.27	0.51	0.47	0.62	0.95	1.59	1.93	2.07
*, **	HRS0	0.61	0.77	1.06	0.50	0.29	0.42	0.75	1.37	1.70	1.83
Section A Cumulative											
	Unit	Mode	Average SR	Median	Standard dev	P5	P13	P32	P68	P87	P95
	HRS3	0.30	0.38	0.54	0.27	0.12	0.20	0.37	0.71	0.89	0.96
	HRS2	0.59	0.62	0.68	0.21	0.34	0.40	0.54	0.81	0.95	1.01
	HRS1	0.99	1.19	1.47	0.58	0.56	0.72	1.11	1.83	2.21	2.38
**	HRS0	0.55	0.77	0.89	0.24	0.52	0.59	0.74	1.03	1.19	1.25
Section B											
Fault F1B	Unit	Mode	Average	Median	Standard dev	P5	P13	P32	P68	P87	P95
	HRS3	–	–	–	–	–	–	–	–	–	–
	HRS2	0.05	0.05	0.06	0.03	0.02	0.02	0.04	0.08	0.10	0.11
	HRS1	0.16	0.19	0.37	0.35	0.00	0.00	0.15	0.59	0.83	0.92
	HRS0	0.53	0.74	0.85	0.23	0.50	0.56	0.71	1.00	1.15	1.21
Fault F2B	Unit	Mode	Average	Median	Standard dev	P5	P13	P32	P68	P87	P95
***	HRS3	0.19	0.23	0.54	0.47	0.00	0.00	0.24	0.83	1.14	1.27
	HRS2	0.08	0.08	0.11	0.11	0.00	0.00	0.05	0.18	0.25	0.28
	HRS1	0.20	0.23	0.33	0.19	0.03	0.09	0.21	0.45	0.57	0.62
	HRS0	0.34	0.43	0.59	0.27	0.17	0.24	0.42	0.75	0.93	1.01
Section B Cumulative											
	Unit	Mode	Average	Median	Standard dev	P5	P13	P32	P68	P87	P95
	HRS3	0.19	0.23	0.54	0.47	0.00	0.00	0.24	0.83	1.14	1.27
	HRS2	0.13	0.14	0.17	0.11	0.00	0.02	0.10	0.24	0.32	0.35
	HRS1	0.37	0.41	0.64	0.43	0.00	0.09	0.37	0.91	1.19	1.31
	HRS0	0.87	1.17	1.41	0.46	0.70	0.83	1.13	1.70	2.00	2.13

* cumulative of F1A and F2A, ** minimum due to erosion, *** cumulative of F2A and F2B

1.8 Myr. To allow a gross comparison with the previous results, we computed the average slip rate values for the San Colombano Structure (SCS) and Casalpusterlengo-Zorlesco Structure (CZS) considering the total displacement cumulated in the last 2.4 Myr from the values reported in Table 3. The results indicate an average slip rate of 0.63 mm/yr for SCS in Section A (Fig. 8) and 0.53 mm/yr for CZS in Section B.

Boccaletti et al. (2011) used published seismic cross-sections (Boccaletti et al., 2004; Cassano et al., 1986; Pieri and Groppi, 1981), measuring the displacement associated with the main structures recorded at the base of Pliocene deposits (5.4 Ma) and that of Pleistocene deposits (1.8 Ma according to the time-scale available at the time of publication). The estimates of slip rates proposed by Boccaletti et al. (2011) indicate 1.5 mm/yr in the last 1.8 Myr as rake-parallel slip rates value but did not consider the differential compaction effect. Maesano et al. (2015) proposed slip rate values obtained with an approach comparable to the one adopted in this study since, in both cases, the effect of the differential compaction was accounted for before the restoration. However, time resolutions in Maesano et al. (2015) and in Boccaletti et al. (2011) were similar, with constraints available only for the Calabrian (1.8 Ma) and Zanclean (5.3 Ma). The results of Maesano et al. (2015) for the Emilia Arc referred to two cross-sections, one located in the western part of the Emilia Arc and one coincident with the geological Section of Fig. 1-D, crossing the eastern segment of the Emilia Arc. The slip rates values obtained by Maesano et al. (2015) are in the order of 0.12 mm/yr in the last 1.8 Myr for the western part of the Emilia Arc, possibly reflecting the along dip component of a lateral ramp with a not negligible horizontal component of motion. The eastern sector shows slip rates in the order of 0.5 mm/yr in the last 1.8 Myr,

comparable with the values computed for the frontal part of the Emilia Arc in this study. The differences between the values proposed in Maesano et al. (2015) and the cumulative value obtained in this study may be explained by the fact that the cross-section used in Maesano et al. (2015) intercepts the Emilia Arc to the east of the main structural culmination. Thus, the slightly lower values of Maesano et al. (2015) may be representative of the lateral variability of the slip rates along the same arc.

Differently from the mentioned works, the approach followed in this study takes into consideration the problem of the non-unique solution provided by the inverse trishear algorithm (Cardozo et al., 2011) by using a result presentation like the ones provided for the Northern Adriatic offshore (Panara et al., 2021). Among the many solutions produced by the inverse trishear restoration, some may have low residuals but may refer to a theoretical fault tip away from the actual fault trace constrained by subsurface data. To overcome this problem, we weighted the various solutions by considering the numerical residual and the distance from the fault. This approach preferentially selects the solutions closer to the fault trace mapped in the geological sections in the slip estimation.

The slip rates presented in this work were estimated by integrating surface and subsurface geological datasets. Similar approaches were used on the foothill of the Northern Apennines (Gunderson et al., 2018; Gunderson et al., 2014; Gunderson et al., 2013; Ponza et al., 2010; Maestrelli et al., 2018) and in the isolated reliefs of Romanengo (Bresciani and Perotti, 2014) and Capriano del Colle (Livio et al., 2009) in the Southern Alps. The outcropping or sub-outcropping thrusts (or thrust splays) of the Northern Apennines foothills show uplift rates of 0.3 mm/
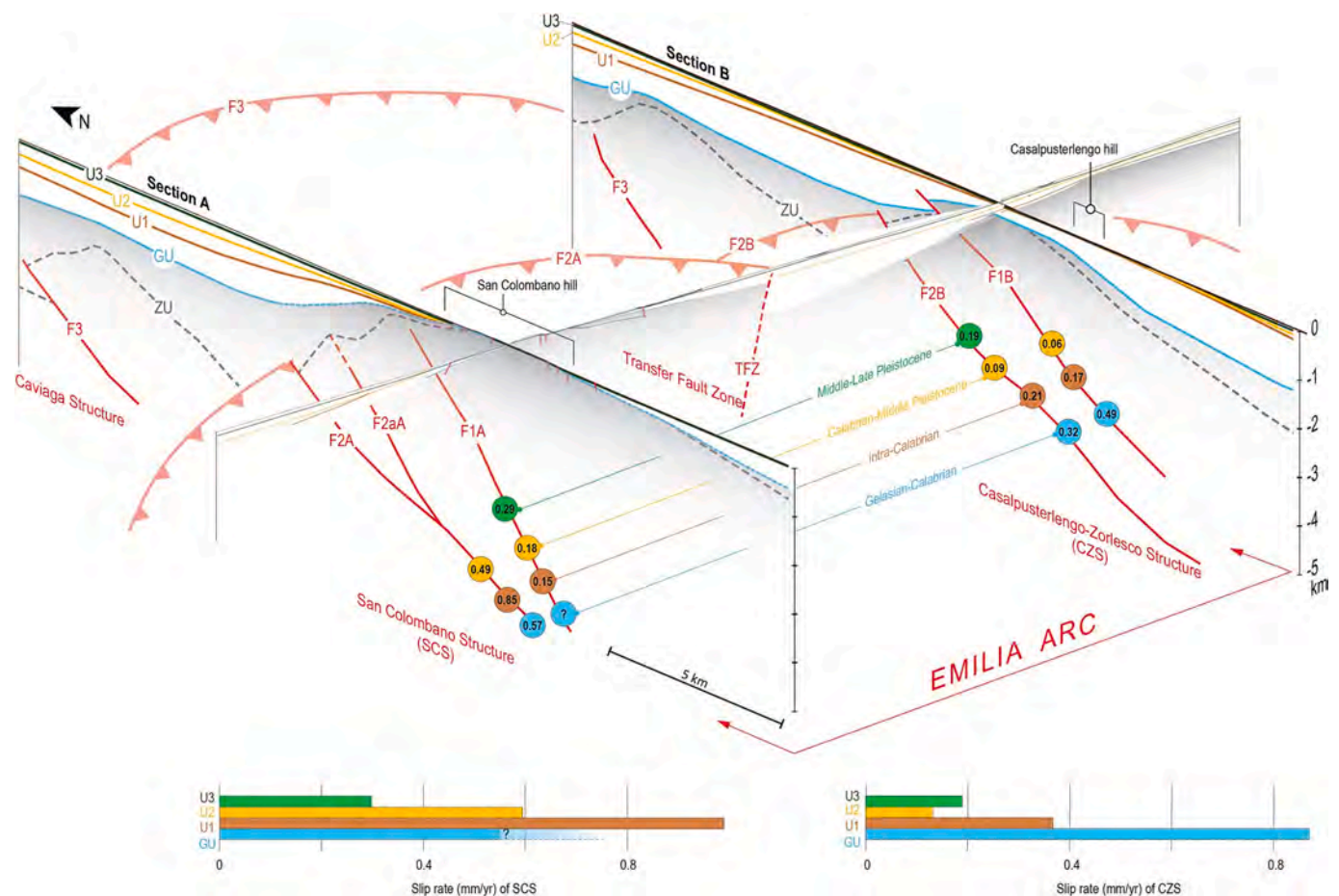
Fig. 9. Quaternary deformation history of the San Colombano (SCS) and Casalpusterlengo-Zorlesco (CZS) Structures, outlined by slip rates mode values calculated for the single faults. At the bottom: histogram of cumulative slip rates for each structure, showing the mode values of thrusts activity during the formation of the four high-rank unconformities (GU, U1, U2, U3). Uncertainty on the slip rate related to GU at the SCS: minimum due to erosion at the hilltop (see text for discussion).

yr in the Broni-Stradella structure, a few kilometres to the south of our study area, based on geomorphological analysis of uplifted river markers (Benedetti et al., 2003). The Salsomaggiore anticline, located southeast of SCS and CZS, shows decreasing slip rates from 6 to 0.1 mm/yr in the last 6 Myr (Gunderson et al., 2013). The morphometric analysis of river incision across the pedeappenninc thrust front between Modena and Reggio Emilia provided uplift rates in the range of 0.18–0.24 mm/yr in the last 620 kyr (Ponza et al., 2010), whereas the slip rates calculated for the same areas using a trishear forward modelling are in the order of 0.7–0.8 mm/yr in a variable period between the last 1.4–0.8 Myr (Maestrelli et al., 2018). The latter work did not consider the effect of differential sediment compaction across folded stratigraphic units and thus may have overestimated 30–40% of the slip required for the deformation according to the synthetic test performed for this study (Supplementary Information Table S1) and with previous studies (Taylor et al., 2008; Maesano et al., 2015; Pizzi et al., 2020).

One of the main improvements proposed in this study is the probabilistic approach to geological data elaboration. Following the work by Zechar and Frankel (2009), we included all the known sources of uncertainty both in the numerator (slip estimation) and in the denominator (time interval). We computed the probabilistic distribution of the slip rates for each stratigraphic unit and relative time interval. This approach has significant implications when using these results as input data in earthquake hazard applications (see Morell et al., 2020, for an overview of this topic).

Most of the current uncertainty relates to the difficulty in age estimation; in particular, the slip rates recorded on the time interval for the deposition of the Calabrian HRS1, in both sections and for all the studied faults, have systematically higher standard deviation compared to the mode and average values (Table 3). The high standard deviation is due to the significant uncertainties in defining the age of the top (U2) and bottom (U1) horizons of HRS1; one reason is the progressive and composite nature of the target stratigraphic boundaries (Zuffetti and Bersezio, 2021), that are time-transgressive surfaces. Moreover, the onset of deposition of the oldest and deepest stratigraphic units (HRS1, HRS2; Fig. 3), might be underestimated because age determinations at their depocenters are lacking. In general, previous works (Bird, 2007; Zechar and Frankel, 2009) suggest that slip rate values may be considered well-constrained if the width of its 95% confidence interval is smaller than the median. Although this is not the case for the values presented in this work, it can be noted that the uncertainty on slip values is, in many cases, relatively low compared to the total slip. Thus, the considerable uncertainty depends mainly on the age constraints. To provide more constrained slip rate values, we stress that further studies should focus on reducing the uncertainty in estimating the timing of the Quaternary unconformities and interposed sediment packages.

Despite the limitations mentioned above, the probabilistic distribution of slip rates presented here shows that for the most recent horizons, there is often a probability of null slip rates due to the low values of measured slip. This consideration suggests that the evidence of recent activity of these faults is quite elusive and difficult to resolve using only low-resolution data. As an example, the offshore blind thrusts of the Northern Apennines front in the Adriatic Sea were considered inactive (Di Bucci and Mazzoli, 2002) based on the analysis of low-resolution data available at the time. The 2022 seismic sequence, which occurred on a blind thrust of the Northern Apennines thrust front in the Adriatic

offshore, demonstrated that these structures were instead active and seismogenic (Maesano et al., 2023). High-resolution geophysical data and robust dating of seismostratigraphic markers may help better define a buried fault's current activity state.

The results show that the slip rates of the San Colombano Structure (SCS) and Casalpusterlengo-Zorlesco Structure (CZS) of the Emilia Arc (Fig. 1) generally slow down during the Quaternary (Fig. 9), in accordance with the other structures of the Northern Apennines thrust front both in the inner part of the Po Plain (Toscani et al., 2009; Boccaletti et al., 2011; Gunderson et al., 2013, 2018) and in the outermost front of the Adriatic Sea (Panara et al., 2021). By summing the displacement values for each section, it is straightforward to notice that not all the deformation related to the thrust development is recovered (total displacement on the top Oligocene horizon of ca. 5700 m measured on regional sections, see Section in Fig. 1-D), but only the 26% and 22% for Section A and Section B respectively. As a consequence, we can state that most of the fault activity occurs in the first stages of thrust development, which dates back to the late Miocene (Ghielmi et al., 2013) in agreement with what was observed in the Northern Adriatic offshore, where most of the buried thrust of the Northern Apennines had their highest slip rates in their early stages of development (Panara et al., 2021), regardless of the specific age of inception.

We can observe the different behaviour in the evolution of the adjacent SCS and CZS by comparing the displacement during the various time intervals obtained by the slip rates analysis. The slip rates during the deposition of the late Calabrian HRS1 are significantly higher at SCS. In contrast, CZS has higher slip rates between Gelasian Unconformity (GU) and Intra-Calabrian Unconformity (U1), even if for the same period, the slip rates computed for SCS should be considered as a minimum due to erosion. This observation suggests a similar evolution of SCS and CZS during their early stages (Miocene and Pliocene) and a predominance of SCS after the deposition of the Calabrian HRS1.

The comparison of the slip necessary for recovering the deformation of Early-Middle Pleistocene Unconformity (U2) between Section A and Section B also indicates that during the deposition of HRS2, SCS recorded higher strain if compared to CZS. This observation suggests a non-synchronous evolution of the two thrust systems during the Quaternary, as Zuffetti and Bersezio (2021) have already proposed by inspecting the shallow 3D subsurface stratigraphic model. The formation of a synformal depocentre for the high-rank HRS2 between the SCS and the CZS (Fig. 3-B) marks the beginning of the separation between the two structures since the end of the Calabrian, accommodated by assuming dextral slip along a NW-SE trending Transfer Fault Zone or lateral ramp of the SCS (TFZ, Fig. 3-B, Fig. 9). Surface geology suggests that from this time and onwards, wrenching, uplift, fold hinge extension and subsequent collapse affected the SCS, giving origin to sets of conjugate normal faults that accompanied its raising above the CZS (Zuffetti and Bersezio, 2020, 2021). These faults displace the GU (Fig. 3-C and Fig. 4-A), but there is no evident cross-cutting relationship with the buried F1A thrust. We interpreted these secondary normal faults as shallow outer arc extensional features. Thus, even if no direct evidence is available, these normal faults should be confined within the hanging wall of SCS (Fig. 3 and Fig. 4-A).

The faults of the Casalpusterlengo-Zorlesco Structure (CZS, Section B) have less evidence of deformation after the deposition of HRS3 compared with the San Colombano Structure (SCS, section A). This observation agrees with the buried setting of the anticline top in the Casalpusterlengo-Zorlesco area and the outcropping fold hinge in the San Colombano hill. On the contrary, the overall displacement recorded at CZS in Section B for HRS0 is higher compared to Section A at SCS. However, this relative anomaly depends on the partial erosion of HRS0 correspondence with the uplifted San Colombano hill, where the Miocene substratum crops out. This observation also reinforces the quantitative results of higher slip rates for SCS compared to CZS.

Concerning the Late Pleistocene deformation stage, it is worth noting that the slip rates mode for HRS3 at the SCS is comparable to the uplift

rate value obtained for the Stradella structure (Benedetti et al., 2003). In addition, the relatively higher slip values of F1A than of F2A faults of the San Colombano Structure (Fig. 6; Table 2; Fig. 9) hold with the interpretation by Zuffetti and Bersezio (2021), who suggested the out-of-sequence propagation of the San Colombano ramp-anticline, where during the Late Pleistocene the deformation concentrated on the inner structure (F1A) instead of the frontal thrust (F2A).

The comparison between the estimated slip rates and the internal stratigraphic architecture of the Quaternary high-rank stratigraphic units suggests some more considerations. For example, the slip rate of 0.13 mm/yr measured at CZS during the Early-Middle Pleistocene relates to the time of formation of unconformity U2, that bounds the Calabrian-Middle Pleistocene HRS2 (Fig. 3-B; Table 3, section B). The intermediate- and low-rank stratigraphic units composing HRS2 (Fig. 3-B) progressively wedge out and lap onto U2 toward the culmination of the CZS ramp anticline at low-angle, testifying that the cumulative slip is the sum of tectonic-depositional increments detectable by the stratigraphic relationships (Zuffetti and Bersezio, 2021). Also, the 3D internal architecture of the Middle-Late Pleistocene HRS3 above unconformity U3 (Fig. 3-B) and the Middle-Late Pleistocene landscape evolution at the SCS (Zuffetti and Bersezio, 2020) suggest that the corresponding estimate of slip rate (0.30 mm/yr, section A, Table 3) might result from the sum of pulse and rest increments (Zuffetti and Bersezio, 2021).

8. Conclusions

This work proposes the probabilistic distribution of the slip rates of the San Colombano Structure (SCS) and Casalpusterlengo-Zorlesco Structure (CZS) composing the Emilia Arc of the Northern Apennines in the central-southern Po plain of Italy during Quaternary. The study was based on a multiscale approach, integrating surface and subsurface datasets describing the 3D subsurface architecture and the evolution of the Quaternary stratigraphic units and buried thrusts of this slowly and mildly deforming thrust front. The results suggest the following remarks:

- Based on the total displacement, the computed average cumulated slip rate values in the last 2.4 Myr are 0.63 mm/yr for SCS and 0.53 mm/yr for CZS. The structures register a general slow-down of the deformation during the Quaternary.
- Although the SCS and CZS record a general slowing of deformation during the Quaternary, they show different growth rates. The faults of the CZS registered higher slip rates during the Early Pleistocene between the Gelasian Unconformity (GU) and the Intra-Calabrian Unconformity (U1), followed by a pronounced slowing at the end of Calabrian. Conversely, the faults of the SCS showed higher values starting from the same period, suggesting that since the end of the Calabrian, the two segments of the Emilia Arc separated, and dextral wrenching and uplift of the SCS occurred along a NW-SE trending transfer fault zone between the two structures.
- The CZS shows minor evidence of deformation during the formation of Middle-Late Pleistocene Unconformity (U3) if compared to the SCS. In this stage, the slip values of the southern faults of the SCS suggest an out-of-sequence propagation of the San Colombano ramp-anticline during the Late Pleistocene.
- The proposed 3D subsurface geological and structural model integrates surface and subsurface stratigraphy based on down-tracing from geological maps, field geological reconstruction, and regional deep subsurface reconstructions based on seismic reflection profiles. The geometry of sedimentary units and bounding unconformities were composed in a hierarchic framework. The chronological data constrain the decompaction and restoration workflow to compute the probabilistic distribution of the slip rates for each stratigraphic unit and relative time interval. The average slip rates obtained in this work are in good accordance with the Quaternary slip rates computed on other buried thrusts in the Po Plain, where surface geological constraints were lacking.

- The adopted probabilistic approach highlights the heterogeneous partition of the deformation along the Emilia Arc front during the Quaternary that has compelling implications when using the results as input data in earthquake hazard applications.

CRediT authorship contribution statement

F.E. Maesano: Writing – review & editing, Writing – original draft, Visualization, Methodology, Investigation, Formal analysis, Data curation, Conceptualization. **C. Zuffetti:** Writing – review & editing, Writing – original draft, Visualization, Formal analysis, Data curation, Conceptualization. **A. Abbate:** Software, Methodology. **C. D'Ambrogi:** Writing – review & editing, Writing – original draft, Visualization, Formal analysis, Data curation, Conceptualization. **R. Bersezio:** Writing – review & editing, Writing – original draft, Conceptualization.

Declaration of competing interest

The authors declare that they have no known competing financial interests or personal relationships that could have appeared to influence the work reported in this paper.

Data availability

The original version of the seismic profile "Appennino – Centrale 1" shown in Fig. 3 can be downloaded from the ViDEPI database: https://www.videpi.com/deposito/videpi/allegati/6645.pdf

The 3D geological subsurface model used in this study (D'Ambrogi et al., 2023) can be downloaded as OGC API - Feature standard at: http://sgi3.isprambiente.it/geoserver_api/ogc/features/collections? f=text%2Fhtml

Acknowledgements

Appendix A. Supplementary data

Supplementary data to this article can be found online at https://doi.org/10.1016/j.tecto.2024.230227.

References

Allen, P.A., Allen, J.R., 2013. Basin Analysis: Principles and Application to Petroleum Play Assessment. John Wiley & Sons.

Allmendinger, R.W., 1998. Inverse and forward numerical modeling of trishear fault-propagation folds. Tectonics 17, 640–656. https://doi.org/10.1029/98TC01907.

Allmendinger, R.W., Cardozo, N., Fisher, D.M., 2011. Structural Geology Algorithms: Vectors and Tensors. Cambridge University Press.

Amadori, C., Toscani, G., Di Giulio, A., Maesano, F.E., D'Ambrogi, C., Ghielmi, M., Fantoni, R., 2019. From cylindrical to non-cylindrical foreland basin: Pliocene–Pleistocene evolution of the Po Plain–Northern Adriatic basin (Italy). Basin Res. 31, 991–1015. https://doi.org/10.1111/bre.12369.

Amorosi, A., Bruno, L., Campo, B., Costagli, B., Hong, W., Picotti, V., Vaiani, S.C., 2021. Deformation patterns of upper Quaternary strata and their relation to active tectonics, Po Basin, Italy. Sedimentology 68, 402–424.

Benedetti, L.C., Tapponnier, P., Gaudemer, Y., Manighetti, I., Van der Woerd, J., 2003. Geomorphic evidence for an emergent active thrust along the edge of the Po Plain: the Broni-Stradella fault. J. Geophys. Res. 108 https://doi.org/10.1029/2001JB001546.

Berberian, M., 1995. Master "blind" thrust faults hidden under the Zagros folds: active basement tectonics and surface morphotectonics. Tectonophysics 241, 193–224. https://doi.org/10.1016/0040-1951(94)00185-C.

Bigi, G., Castellarin, A., Coli, M., Dal Piaz, G.V., Sartori, R., Scandone, P., Vai, G.B., 1992. Structural Model of Italy Scale 1:500.000, Sheet 1.

Bini, A., Baio, M., Violanti, D., Martinetto, E., 2016. Nuovi dati da sondaggi provenienti dai dintorni di San Colombano al Lambro e dalla Pianura Padana a Est di Milano: analisi litostratigrafica, composizionale e micropaleontologica. Geol. Insubrica 12.

Bird, P., 2007. Uncertainties in long-term geologic offset rates of faults: General principles illustrated with data from California and other western states. Geosphere 3, 577–595. https://doi.org/10.1130/GES00127.1.

Boccaletti, M., Bonini, M., Corti, G., Gasperini, P., Martelli, L., Piccardi, L., Tanini, C., Vannucci, G., 2004. Seismotectonic Map of the Emilia-Romagna Region. Regione Emilia Romagna & SELCA, Firenze, Italy.

Boccaletti, M., Corti, G., Martelli, L., 2011. Recent and active tectonics of the external zone of the Northern Apennines (Italy). Int J Earth Sci (Geol Rundsch) 100, 1331–1348. https://doi.org/10.1007/s00531-010-0545-y.

Bonini, L., Toscani, G., Seno, S., 2014. Three-dimensional segmentation and different rupture behavior during the 2012 Emilia seismic sequence (Northern Italy). Tectonophysics 630, 33–42. https://doi.org/10.1016/j.tecto.2014.05.006.

Bresciani, I., Perotti, C.R., 2014. An active deformation structure in the Po Plain (N Italy): the Romanengo anticline. Tectonics 33, 2059–2076. https://doi.org/10.1002/2013TC003422.

Burrato, P., Ciucci, F., Valensise, G., 2003. An inventory of river anomalies in the Po Plain, Northern Italy: evidence for active blind thrust faulting. Annals of Geophysics 46. https://doi.org/10.4401/ag-3459.

Burrato, P., Vannoli, P., Fracassi, U., Basili, R., Valensise, G., 2012. Is blind faulting truly invisible? Tectonic-controlled drainage evolution in the epicentral area of the May 2012, Emilia-Romagna earthquake sequence (northern Italy). Ann. Geophys. 55 https://doi.org/10.4401/ag-6182.

Buttinelli, M., Maesano, F.E., Sopher, D., Feriozzi, F., Maraio, S., Mazzarini, F., Improta, L., Vallone, R., Villani, F., Basili, R., 2022. Revitalising vintage seismic reflection profiles by converting into SEG-Y format: case studies from publicly available data on the Italian territory. Annals of Geophysics 65, DM538. https://doi.org/10.4401/ag-8883.

Campo, B., Bruno, L., Amorosi, A., 2020. Basin-scale stratigraphic correlation of late Pleistocene-Holocene (MIS 5e-MIS 1) strata across the rapidly subsiding Po Basin (northern Italy). Quat. Sci. Rev. 237, 106300 https://doi.org/10.1016/j.quascirev.2020.106300.

Cardozo, N., Jackson, C.A.-L., Whipp, P.S., 2011. Determining the uniqueness of best-fit trishear models. Journal of Structural Geology 33, 1063–1078. https://doi.org/10.1016/j.jsg.2011.04.001.

Carminati, E., Doglioni, C., 2012. Alps vs. Apennines: the paradigm of a tectonically asymmetric Earth. Earth Sci. Rev. 112, 67–96. https://doi.org/10.1016/j.earscirev.2012.02.004.

Carminati, E., Doglioni, C., Scrocca, D., 2003. Apennines subduction-related subsidence of Venice (Italy). Geophys. Res. Lett. 30 https://doi.org/10.1029/2003GL017001.

Cassano, E., Anelli, L., Fichera, R., Cappelli, V., 1986. Pianura Padana: Interpretazione integrata di dati geofisici e geologici. In: Presented at the 73° Congresso Società Geologica Italiana, AGIP, Roma, p. 27.

Cohen, K.M., Gibbard, P.L., 2019. Global chronostratigraphical correlation table for the last 2.7 million years, version 2019 QI-500. Quat. Int. 500, 20–31.

Crippa, G., Baucon, A., Felletti, F., Raineri, G., Scarponi, D., 2018. A multidisciplinary study of ecosystem evolution through early Pleistocene climate change from the marine Arda River section, Italy. Quatern. Res. 89, 533–562.

D'Ambrogi, C., Maesano, F.E., Marino, M., Congi, M.P., Morrone, S., 2023. Geological 3D model of the Po Basin. https://doi.org/10.15161/OAR.IT/76873.

Danciu, L., Weatherill, G., Rovida, A., Basili, R., Bard, P.-Y., Beauval, C., Nandan, S., Pagani, M., Crowley, H., Sesetyan, K., Villanova, S., Reyes, C., Marti, M., Cotton, F., Wiemer, S., Giardini, D., 2022. The 2020 European Seismic Hazard Model: Milestones and Lessons Learned. In: Vacareanu, R., Ionescu, C. (Eds.), Progresses in European Earthquake Engineering and Seismology. Springer Proceedings in Earth and Environmental Sciences. Springer International Publishing, Cham, pp. 3–25. https://doi.org/10.1007/978-3-031-15104-0_1.

Desio, A., 1965. I rilievi isolati della Pianura Lombarda ed i movimenti tettonici del Quaternario. Rend Ist Lom Acc Sc Lett, Sez A 99, 881–894.

Devoti, R., Esposito, A., Pietrantonio, G., Pisani, A.R., Riguzzi, F., 2011. Evidence of large scale deformation patterns from GPS data in the Italian subduction boundary. Earth Planet. Sci. Lett. 311, 230–241. https://doi.org/10.1016/j.epsl.2011.09.034.

Di Bucci, D., Mazzoli, S., 2002. Active tectonics of the Northern Apennines and Adria geodynamics: new data and a discussion. J. Geodyn. 34, 687–707. https://doi.org/10.1016/S0264-3707(02)00107-2.

DISS Working Group, 2021. Database of Individual Seismogenic Sources (DISS), version 3.3.0: A compilation of potential sources for earthquakes larger than M 5.5 in Italy and surrounding areas. 132 Individual Seismogenic Sources, 197 Composite Seismogenic Sources, 38 Debated Seismogenic Sources, 4 Subduction Zones. https://doi.org/10.13127/DISS3.3.0.

Doski, J.A.H., 2021. Active tectonics along the Sheladiz seismogenic fault in the Western Zagros fold-thrust belt, Kurdistan, Northern Iraq. Int J Earth Sci (Geol Rundsch) 110, 595–608. https://doi.org/10.1007/s00531-020-01973-y.

Egan, S.S., Kane, S., Buddin, T.S., Williams, G.D., Hodgetts, D., 1999. Computer modelling and visualisation of the structural deformation caused by movement along geological faults. Comput. Geosci. 25, 283–297. https://doi.org/10.1016/S0098-3004(98)00125-3.

Erslev, E.A., 1991. Trishear fault-propagation folding. Geology 19, 617–620. https://doi.org/10.1130/0091-7613(1991)019<0617:TFPF>2.3.CO;2.

Fantoni, R., Franciosi, R., 2010. Tectono-sedimentary setting of the Po Plain and Adriatic foreland. Rend. Fis. Acc. Lincei 21, 197–209. https://doi.org/10.1007/s12210-010-0102-4.

Fantoni, R., Bersezio, R., Forcella, F., 2004. Alpine structure and deformation chronology at the southern Alps-Po Plain border in Lombardy. Italian Journal of Geosciences 123, 463–476.

Ghielmi, M., Minervini, M., Nini, C., Rogledi, S., Rossi, M., Vignolo, A., 2010. Sedimentary and tectonic evolution in the eastern Po-Plain and northern Adriatic Sea area from Messinian to Middle Pleistocene (Italy). Rend. Fis. Acc. Lincei 21, 131–166. https://doi.org/10.1007/s12210-010-0101-5.

Ghielmi, M., Minervini, M., Nini, C., Rogledi, S., Rossi, M., 2013. Late Miocene–Middle Pleistocene sequences in the Po Plain – Northern Adriatic Sea (Italy): The stratigraphic record of modification phases affecting a complex foreland basin. Marine and Petroleum Geology 42, 50–81. https://doi.org/10.1016/j.marpetgeo.2012.11.007.

Gold, R.D., Cowgill, E., Wang, X.-F., Chen, X.-H., 2006. Application of trishear fault-propagation folding to active reverse faults: examples from the Dalong Fault, Gansu Province, NW China. J. Struct. Geol. 28, 200–219. https://doi.org/10.1016/j.jsg.2005.10.006.

Guidoboni, E., Comastri, A., Boschi, E., 2005. The "exceptional" earthquake of 3 January 1117 in the Verona area (northern Italy): a critical time review and detection of two lost earthquakes (lower Germany and Tuscany). J. Geophys. Res. Solid Earth 110. https://doi.org/10.1029/2005JB003683.

Gunderson, K.L., Anastasio, D.J., Pazzaglia, F.J., Picotti, V., 2013. Fault slip rate variability on 104–105yr timescales for the Salsomaggiore blind thrust fault, Northern Apennines, Italy. Tectonophysics 608, 356–365. https://doi.org/10.1016/j.tecto.2013.09.018.

Gunderson, K.L., Pazzaglia, F.J., Picotti, V., Anastasio, D.A., Kodama, K.P., Rittenour, T., Frankel, K.F., Ponza, A., Berti, C., Negri, A., Sabbatini, A., 2014. Unraveling tectonic and climatic controls on synorogenic growth strata (Northern Apennines, Italy). Geol. Soc. Am. Bull. 126, 532–552. https://doi.org/10.1130/B30902.1.

Gunderson, K.L., Anastasio, D.J., Pazzaglia, F.J., Kodama, K.P., 2018. Intrinsically Variable Blind Thrust Faulting. Tectonics 37, 1454–1471. https://doi.org/10.1029/2017TC004917.

Improta, L., Cirella, A., Pezzo, G., Molinari, I., Piatanesi, A., 2023. Joint Inversion of Geodetic and strong Motion Data for the 2012, Mw 6.1–6.0, May 20th and May 29th, Northern Italy Earthquakes: Source Models and Seismotectonic Interpretation. Journal of Geophysical Research: Solid Earth 128. https://doi.org/10.1029/2022JB026278 e2022JB026278.

ISPRA, 2015. Modello geologico 3D e geopotenziali della Pianura Padana centrale (Progetto GeoMol), Rapporti ISPRA.

Johnson, C.S., Miller, K.G., Browning, J.V., Kopp, R.E., Khan, N.S., Fan, Y., Stanford, S. D., Horton, B.P., 2018. The role of sediment compaction and groundwater withdrawal in local sea-level rise, Sandy Hook, New Jersey, USA. Quaternary Science Reviews 181, 30–42. https://doi.org/10.1016/j.quascirev.2017.11.031.

Latorre, D., Raffaele, D.S., Barbara, C., Maddalena, M., Lauro, C., 2023. An updated view of the Italian seismicity from probabilistic location in 3D velocity models: the 1981–2018 Italian catalog of absolute earthquake locations (CLASS). Tectonophysics 846, 229664. https://doi.org/10.1016/j.tecto.2022.229664.

Livani, M., Scrocca, D., Arecco, P., Doglioni, C., 2018. Structural and Stratigraphic Control on Salient and recess Development along a Thrust Belt Front: the Northern Apennines (Po Plain, Italy). J. Geophys. Res. Solid Earth 123, 4360–4387. https://doi.org/10.1002/2017JB015235.

Livio, F.A., Berlusconi, A., Michetti, A.M., Sileo, G., Zerboni, A., Trombino, L., Cremaschi, M., Mueller, K., Vittori, E., Carcano, C., Rogledi, S., 2009. Active fault-related folding in the epicentral area of the December 25, 1222 (Io=IX MCS) Brescia earthquake (Northern Italy): Seismotectonic implications. Tectonophysics 476, 320–335. https://doi.org/10.1016/j.tecto.2009.03.019.

Locati, M., Camassi, R., Rovida, A., Ercolani, E., Bernardini, F., Castelli, V., Caracciolo, C. H., Tertulliani, A., Rossi, A., Azzaro, R., D'Amico, S., Antonucci, A., 2022. Database Macrosismico Italiano (DBMI15), versione 4.0. https://doi.org/10.13127/DBMI/DBMI15.4.

Maesano, F.E., D'Ambrogi, C., 2017. Vel-IO 3D: a tool for 3D velocity model construction, optimization and time-depth conversion in 3D geological modeling workflow. Comput. Geosci. 99, 171–182. https://doi.org/10.1016/j.cageo.2016.11.013.

Maesano, F.E., Toscani, G., Burrato, P., Mirabella, F., D'Ambrogi, C., Basili, R., 2013. Deriving thrust fault slip rates from geological modeling: examples from the Marche coastal and offshore contraction belt, Northern Apennines, Italy. Marine and Petroleum Geology 42, 122–134. https://doi.org/10.1016/j.marpetgeo.2012.10.008.

Maesano, F.E., D'Ambrogi, C., Burrato, P., Toscani, G., 2015. Slip-rates of blind thrusts in slow deforming areas: examples from the Po Plain (Italy). Tectonophysics 643, 8–25. https://doi.org/10.1016/j.tecto.2014.12.007.

Maesano, F.E., Buttinelli, M., Maffucci, R., Toscani, G., Basili, R., Bonini, L., Burrato, P., Fedorik, J., Fracassi, U., Panara, Y., Tarabusi, G., Tiberti, M.M., Valensise, G., Vallone, R., Vannoli, P., 2023. Buried Alive: Imaging the 9 November 2022, Mw 5.5 Earthquake Source on the Offshore Adriatic Blind Thrust Front of the Northern Apennines (Italy). Geophysical Research Letters 50. https://doi.org/10.1029/2022GL102299 e2022GL102299.

Maestrelli, D., Benvenuti, M., Bonini, M., Carnicelli, S., Piccardi, L., Sani, F., 2018. The structural hinge of a chain-foreland basin: Quaternary activity of the Pede-Apennine Thrust front (Northern Italy). Tectonophysics 723, 117–135. https://doi.org/10.1016/j.tecto.2017.12.006.

Malagnini, L., Herrmann, R.B., Munafò, I., Buttinelli, M., Anselmi, M., Akinci, A., Boschi, E., 2012. The 2012 Ferrara seismic sequence: Regional crustal structure, earthquake sources, and seismic hazard. Geophys. Res. Lett. 39 https://doi.org/10.1029/2012GL053214.

Mele, M., Inzoli, S., Giudici, M., Bersezio, R., 2014. Relating electrical conduction of alluvial sediments to textural properties and pore-fluid conductivity: Experimental study of electrical conduction of sediments. Geophys. Prospect. 62, 631–645. https://doi.org/10.1111/1365-2478.12102.

Mele, M., Bersezio, R., Giudici, M., 2018. An electrostratigraphic cross-section across the Central Po plain: bearings on subsurface geology and hydrostratigraphy. Int J Earth Sci (Geol Rundsch) 107, 2787–2802. https://doi.org/10.1007/s00531-018-1627-5.

Meletti, C., Marzocchi, W., D'Amico, V., Lanzano, G., Luzi, L., Martinelli, F., Pace, B., Rovida, A., Taroni, M., Visini, F., Group, M.W, 2021. The new Italian seismic hazard model (MPS19). Annals of Geophysics 64. https://doi.org/10.4401/ag-8579. SE112–SE112.

Moore, P.D., Webb, J.A., Collison, M.E., 1991. Pollen Analysis. Blackwell scientific publications.

Morell, K.D., Styron, R., Stirling, M., Griffin, J., Archuleta, R., Onur, T., 2020. Seismic Hazard analyses from geologic and geomorphic data: current and Future challenges. Tectonics 39. https://doi.org/10.1029/2018TC005365 e2018TC005365.

Muttoni, G., Carcano, C., Garzanti, E., Ghielmi, M., Piccin, A., Pini, R., Rogledi, S., Sciunnach, D., 2003. Onset of major Pleistocene glaciations in the Alps. Geol 31, 989. https://doi.org/10.1130/G19445.1.

Myers, D.J., Nabelek, J.L., Yeats, R.S., 2003. Dislocation modeling of blind thrusts in the eastern Los Angeles basin, California. J. Geophys. Res. 108 https://doi.org/10.1029/2002JB002150.

Oakley, D.O., Fisher, D.M., 2015. Inverse trishear modeling of bedding dip data using Markov chain Monte Carlo methods. Journal of Structural Geology 80, 157–172.

Panara, Y., Maesano, F.E., Amadori, C., Fedorik, J., Toscani, G., Basili, R., 2021. Probabilistic assessment of slip rates and their variability over time of offshore buried thrusts: a case study in the Northern Adriatic Sea. Frontiers Earth Sci. 9.

Pieri, M., Groppi, G., 1981. Subsurface Geological Structure of the Po Plain, Italy, Prog. Fin. Geodinamica. C.N.R.

Pizzi, M., Lonergan, L., Whittaker, A.C., Mayall, M., 2020. Growth of a thrust fault array in space and time: an example from the deep-water Niger delta. Journal of Structural Geology 137, 104088. https://doi.org/10.1016/j.jsg.2020.104088.

Ponza, A., Pazzaglia, F.J., Picotti, V., 2010. Thrust-fold activity at the mountain front of the Northern Apennines (Italy) from quantitative landscape analysis. Geomorphology 123, 211–231. https://doi.org/10.1016/j.geomorph.2010.06.008.

Rossi, M., Minervini, M., Ghielmi, M., Rogledi, S., 2015. Messinian and Pliocene erosional surfaces in the Po Plain-Adriatic Basin: Insights from allostratigraphy and sequence stratigraphy in assessing play concepts related to accommodation and gateway turnarounds in tectonically active margins. Mar. Pet. Geol. 66, 192–216. https://doi.org/10.1016/j.marpetgeo.2014.12.012.

Rovida, A., Locati, M., Camassi, R., Lolli, B., Gasperini, P., Antonucci, A., 2022. Catalogo Parametrico dei Terremoti Italiani (CPTI15), versione 4.0. https://doi.org/10.13127/CPTI/CPTI15.4.

Sbarra, P., Burrato, P., Tosi, P., Vannoli, P., De Rubeis, V., Valensise, G., 2019. Inferring the depth of pre-instrumental earthquakes from macroseismic intensity data: a case-history from Northern Italy. Sci. Rep. 9, 15583. https://doi.org/10.1038/s41598-019-51966-4.

Sbarra, P., Burrato, P., De Rubeis, V., Tosi, P., Valensise, G., Vallone, R., Vannoli, P., 2023. Inferring the depth and magnitude of pre-instrumental earthquakes from intensity attenuation curves. Nat. Hazards Earth Syst. Sci. 23, 1007–1028. https://doi.org/10.5194/nhess-23-1007-2023.

Scardia, G., De Franco, R., Muttoni, G., Rogledi, S., Caielli, G., Carcano, C., Sciunnach, D., Piccin, A., 2012. Stratigraphic evidence of a Middle Pleistocene climate-driven flexural uplift in the Alps. Tectonics 31. https://doi.org/10.1029/2012TC003108.

Sclater, J.G., Christie, P.A., 1980. Continental stretching: an explanation of the post-mid-cretaceous subsidence of the Central North Sea basin. J. Geophys. Res. Solid Earth 85, 3711–3739.

Scognamiglio, L., Tinti, E., Quintiliani, M., 2006. Time Domain Moment Tensor (TDMT). https://doi.org/10.13127/TDMT.

Scrocca, D., Carminati, E., Doglioni, C., Marcantoni, D., 2007. Slab Retreat and active Shortening along the Central-Northern Apennines. In: Lacombe, O., Roure, F., Lavé, J., Vergés, J. (Eds.), Thrust Belts and Foreland Basins, Frontiers in Earth Sciences. Springer, Berlin, Heidelberg, pp. 471–487. https://doi.org/10.1007/978-3-540-69426-7_25.

Sopher, D., 2018. Converting scanned images of seismic reflection data into SEG-Y format. Earth Sci Inform 11, 241–255. https://doi.org/10.1007/s12145-017-0329-z.

Taylor, S.K., Nicol, A., Walsh, J.J., 2008. Displacement loss on growth faults due to sediment compaction. Journal of Structural Geology 30, 394–405. https://doi.org/10.1016/j.jsg.2007.11.006.

Tibaldi, A., De Nardis, R., Torrese, P., Bressan, S., Pedicini, M., Talone, D., Bonali, F.L., Corti, N., Russo, E., Lavecchia, G., 2023. A multiscale approach to the recent activity of the Stradella thrust in the seismotectonic context of the Emilia Arc (northwestern Italy). Tectonophysics 857, 229853. https://doi.org/10.1016/j.tecto.2023.229853.

Toscani, G., Burrato, P., Di Bucci, D., Seno, S., Valensise, G., 2009. Plio-Quaternary tectonic evolution of the Northern Apennines thrust fronts(Bologna-Ferrara section, Italy): seismotectonic implications. Ital. J. Geosci. 605–613 https://doi.org/10.3301/IJG.2009.128.2.605.

Vannoli, P., Burrato, P., Valensise, G., 2015. The Seismotectonics of the Po Plain (Northern Italy): Tectonic Diversity in a Blind Faulting Domain. Pure Appl. Geophys. 172, 1105–1142. https://doi.org/10.1007/s00024-014-0873-0.

Visini, F., Pace, B., Meletti, C., Marzocchi, W., Akinci, A., Azzaro, R., Barani, S., Barberi, G., Barreca, G., Basili, R., Bird, P., Bonini, M., Burrato, P., Busetti, M., Carafa, M., Cocina, O., Console, R., Corti, G., D'Agostino, N., D'Amico, S., D'Amico, V., Dal Cin, M., Falcone, G., Fracassi, U., Gee, R., Kastelic, V., Lai, C., Langer, H., Maesano, F., Marchesini, A., Martelli, L., Monaco, C., Murru, M., Peruzza, L., Poli, M., Pondrelli, S., Rebez, A., Rotondi, R., Rovida, A., Sani, F., Santulin, M., Scafidi, D., Selva, J., Slejko, D., Spallarossa, D., Tamaro, A., Tarabusi, G., Taroni, M., Tiberti, M., Tusa, G., Tuvè, T., Valensise, G., Vannoli, P., Varini, E., Zanferrari, A., Zuccolo, E., 2021. Earthquake rupture forecasts for the MPS19 seismic hazard model of Italy. Annals of Geophysics 64, 3. https://doi.org/10.4401/ag-8608.

Zechar, J.D., Frankel, K.L., 2009. Incorporating and reporting uncertainties in fault slip rates. J. Geophys. Res. 114, B12407. https://doi.org/10.1029/2009JB006325.

Zuffetti, C., Bersezio, R., 2020. Morphostructural evidence of late Quaternary tectonics at the Po Plain-Northern Apennines border (Lombardy, Italy). Geomorphology 364, 107245. https://doi.org/10.1016/j.geomorph.2020.107245.

Zuffetti, C., Bersezio, R., 2021. Space–time geological model of the Quaternary syntectonic fill of a foreland basin (Po basin, Northern Italy). Sediment. Geol. 421, 105945 https://doi.org/10.1016/j.sedgeo.2021.105945.

Zuffetti, C., Bersezio, R., Contini, D., Petrizzo, M.R., 2018a. Geology of the San Colombano hill, a Quaternary isolated tectonic relief in the Po Plain of Lombardy (Northern Italy). J. Maps 14, 199–211. https://doi.org/10.1080/17445647.2018.1443166.

Zuffetti, C., Trombino, L., Zembo, I., Bersezio, R., 2018b. Soil evolution and origin of landscape in a late Quaternary tectonically mobile setting: the Po Plain-Northern Apennines border in Lombardy (Italy). CATENA 171, 376–397. https://doi.org/10.1016/j.catena.2018.07.026.

Zuffetti, C., Bersezio, R., Trombino, L., 2018c. Significance of the morphological and stratigraphic surfaces in the Quaternary Po Plain: the San Colombano tectonic relief (Lombardy, Italy). Alpine and Mediterranean Quaternary 31, 257–260.

Zuffetti, C., Comunian, A., Bersezio, R., Renard, P., 2020. A new perspective to model subsurface stratigraphy in alluvial hydrogeological basins, introducing geological hierarchy and relative chronology. Comput. Geosci. 140, 104506.